Perivascular M2 Macrophages Stimulate Tumor Relapse after Chemotherapy

Stimulation of Tumor Relapse After Chemotherapy by Perivascular, Alternatively Activated Macrophages

Stimulation of Tumor Relapse After Chemotherapy by Perivascular, Alternatively Activated Macrophages

Russell Hughes[1*], Bin-Zhi Qian[2*] Charlotte Rowan[1], Munitta Muthana[1], Ioanna Keklikoglou[3], Oakley C. Olson[4], Simon Tazzyman[1], Sarah Danson[1], Christina Addison[5], Mark Clemons[5], Ana Maria Gonzalez-Angulo[6] Johanna A. Joyce[4] Michele De Palma[3], Jeffrey W. Pollard[2^] and Claire E. Lewis[1+^]

[1]Departments of Oncology,
University of Sheffield Medical School,
Sheffield, S10 2RX, UK

[2]MRC Centre for Reproductive Health,
Queen's Medical Research Institute,
University of Edinburgh,
Edinburgh EH16 4TJ

[3]Swiss Institute for Experimental Cancer Research (ISREC),
School of Life Sciences, École Polytechnique Fédérale de Lausanne (EPFL),
Lausanne, Switzerland

[4]Cancer Biology and Genetics Program,
Memorial Sloan-Kettering Cancer Center,
New York, NY 10065, USA

[5]Cancer Therapeutics Program,
Ottawa Hospital Research Institute, and Department of Medicine,
University of Ottawa
Ontario, Canada

[6]Breast Medical Oncology
MD Anderson Cancer Center
1515 Holcombe Blvd.
Houston, TX 77030-4009, USA

[*] Co-first authors
[^] Co-senior authors
[+] Corresponding author

Running title: macrophages & tumor relapse
Key words: macrophages, perivascular, M2, relapse, regrowth.

The authors declare no conflicts of interest exist.

Abstract

Tumor relapse after chemotherapy is a major clinical problem, especially for patients with inoperable primary and/or metastatic cancer. Tumor-associated macrophages (TAMs) are known to both promote key steps in tumor progression and to limit the cytotoxic effects of chemotherapeutic agents on mouse tumors. Here, we show that alternatively (M2) activated ($MRC1^{+}TIE2^{Hi}CXCR4^{Hi}$) TAMs accumulate around blood vessels in tumors after chemotherapy and then promote tumor revascularisation and relapse, in part, via their release of VEGFA. Importantly, a similar perivascular, M2-skewed TAM subset was also present in primary human breast carcinomas and bone metastases after chemotherapy. While a small proportion of M2 TAMs were also present in hypoxic tumor areas, when we genetically ablated their ability to respond to hypoxia via hypoxia-inducible factors (HIFs) 1 and 2, tumor relapse was unaffected, further supporting the role of TAMs in well-oxygenated areas in this phenomenon. TAMs were the predominant cells expressing immunoreactive CXCR4 in chemotherapy-treated mouse tumors, with the highest levels expressed by $MRC1^{+}$ TAMs clustering around the tumor vasculature. Furthermore, the primary ligand for CXCR4, CXCL12, was upregulated in these perivascular sites after chemotherapy and shown to be selectively chemotactic for $MRC1^{+}$ TAMs. Finally, pharmacological blockade of CXCR4 selectively reduced the numbers of these M2-skewed TAMs after chemotherapy, especially those in direct contact with blood vessels, resulting in reduced tumor revascularisation and regrowth. These studies highlight a possible new strategy to extend the beneficial effects of chemotherapy - the selective targeting of these perivascular, relapse-promoting M2-skewed TAMs.

Introduction

The regrowth of tumors after treatment with cytotoxic agents poses a major threat to survival in cancer patients, particularly those with inoperable primary and/or metastatic tumors as they often rely heavily on chemotherapy to slow tumor growth and reduce its burden. The development of resistance results in poor survival rates for patients with, for example, inoperable pancreatic or lung cancer, who often survive for less than 12 months after diagnosis (1,2). New therapeutic strategies are, therefore, urgently needed to delay or prevent tumor regrowth after early cycles of chemotherapy as these would extend life.

Malignant tumors contain various $CD11b^+$ myeloid cells including granulocytes, myeloid-derived suppressor cells (MDSCs), and tumor-associated macrophages (TAMs) (3). The latter are recruited as monocytes from the peripheral blood, which are themselves derived from progenitor cells in the bone marrow (4,5). Following entry into tumors, monocytes differentiate into macrophages (6) and promote tumor progression by stimulating tumor invasion, neovascularisation and metastasis, and suppressing anti-tumor immunity (5,7). TAMs express a broad spectrum of activation states between the two extreme forms of 'classical' (M1) and 'alternative' (M2) activation, with a tendency towards the latter (8). M2-skewed TAMs are characterized by their upregulation of various receptors including the mannose receptor C-type lectin (MRC1/CD206) and the angiopoietin receptor, TIE2 (9). Indeed, TAMs expressing high levels of these two receptors have been shown to play an essential role in promoting angiogenesis in untreated mouse tumors (10).

A variety of anti-cancer therapies have been shown to stimulate the recruitment of $CD11b^+$ myeloid cells by mouse tumors (11,12). For example, TAMs accumulate in mouse tumors after chemotherapy (13-15), ionizing radiation (16-18) and the vascular disrupting agent, combretastatin-A4-P (CA-4-P) (19). Importantly, the mononuclear phagocyte growth factor, CSF1 (13), and chemokines, CCL2 (14) and CXCL12 (16,19), are increased in tumors following such anti-cancer therapies, and can trigger monocyte recruitment (4,5). These cells then

reduce the efficacy of chemotherapy by limiting vascular permeability via their expression of MMP9 (14), promoting resistance to therapy-induced death via their expression of cathepsin serine proteases (15) and by suppressing the recruitment/activation of cytotoxic T-cells (12,13).

Considerable evidence has emerged recently for M2-activated macrophages playing an important role in repair and remodelling after tissue injury. For example, they are prominent in diseased tissues in spinal cord injury, myocardial infarction and various forms of renal disease, (20). Furthermore, TAMs with similar phenotypes have been implicated in tumor relapse after therapies like irradiation and CA-4-P (17,19). Although $MRC1^{+}$ TAMs are increased in MMTV-PyMT mammary tumors after doxorubicin treatment (14), the role of M2 TAMs in tumor relapse after chemotherapy has not been defined.

Our studies show that $MRC1^{+}$ TAMs are elevated in mouse tumors after treatment with various chemotherapeutic agents. Moreover, this TAM subset was further defined as $MRC1^{Hi}TIE2^{Hi}CXCR4^{Hi}VEGFA^{+}$ and shown to accumulate preferentially in vascularised, CXCL12-rich regions of tumors after chemotherapy. Blockade of CXCR4 signalling prevented this close association with the tumor vasculature after chemotherapy, resulting in a marked delay in subsequent tumor revascularization and relapse. These findings suggest that selective targeting of vessel-associated, M2-skewed TAMs after chemotherapy could increase the relapse-free survival of cancer patients.

Materials and Methods

Mouse studies

To investigate the mechanisms regulating tumor relapse after chemotherapy, we primarily used the Lewis lung carcinoma model (21) and MMTV-PyMT model of breast cancer (15). These syngeneic tumor models respond to chemotherapy with an initial phase of tumor growth inhibition, followed by a distinct regrowth phase. Transgenic tumor models were not considered suitable as their responses to some cytotoxic agents can be so minimal that a relapse phase is

not evident (13,22). Furthermore, tumors in these models are often multifocal making the kinetics of tumor relapse difficult to assess accurately.

Our mouse studies were conducted in accordance with either UK Home Office regulations (CEL/MM/RH), the Veterinary Authorities of the Canton Vaud (MDP), the institutional standards of the Research Animals Resource Centre at Memorial Sloan-Kettering Cancer Centre (JAJ) and the Albert Einstein College of Medicine Animal Use Committee (JWP). LLC1/CTX studies using 8-week old C57BL/6 mice were performed as described previously (21). For LLC1/AMD3100 studies; AMD3100 was given concurrently (10 mg/Kg) with CTX, i.p. every day for 7 days. Tumors and organs were harvested at the indicated times. Mice were treated i.p. with pimonidazole (60 mg/Kg) and BrdU (100 mg/Kg) 2h prior to sacrifice to label hypoxia and proliferating cells, respectively. 4T1/paclitaxel studies; Female Balb/c mice (>8 weeks) were orthotopically implanted with $1x10^6$ 4T1 murine mammary adenocarcinoma cells. Tumors were grown for 10 days before mice were injected i.p. with either cremaphore or cremophore+PTX (10 mg/kg) every 5 days for a total of 3 doses, the mice were sacrificed and tissues harvested 4 days after the last treatment. Orthotopic MMTV-PyMT/DOX studies were performed as previously described (15). Mice bearing implanted tumors were injected i.v. with a single dose of DOX (5 mg/kg) when at 250 mm^3 and sacrificed 7d post-therapy. Monocyte/macrophage-specific ablation of *Vegfa* studies*:* Female Tg(*Csf1r-Mer-iCre-Mer)*$_{1jwp}$*;Vegfa*$^{fl/fl}$*)* mice (>8weeks), shown to specifically lack the expression of VEGFA in the monocyte/macrophage lineage following treatment with tamoxifen (23), or *Cre* negative litter mates (aged 8 weeks+) were orthotopically implanted with the syngeneic MMTV-PyMT cell line, F246-6. Vegfa floxed mice were the kind gift of Dr Naploeone Ferrar, Genentech. Mice with established tumors were treated with a single i.v. injection of either vehicle (PBS) or DOX (5 mg/Kg) and 24h later with tamoxifen via their food (3mg/20g body weight/day). Treatment with tamoxifen was then maintained throughout tumor regrowth. Tumor growth was monitored by caliper measurements. In the LLC1/TAM adoptive transfer studies, C57BL/6 mice implanted

with LLCs and treated with CTX as outline above, 48h after the last dose of CTX, donor mice were sacrificed, their tumors removed, enzymatically dissociated, and $MRC1^{Hi}$ and $MRC1^{Lo}$ TAMs were purified by flow cytometry. Recipient mice were randomised into three groups and received either 50 $x10^3$ $MRC1^{Hi}$ TAMs, 50 x 10^3 $MRC1^{Lo}$ TAMs, or saline via a 25 µL intra-tumoral injection. Following injection of these cells or saline, tumor re-growth was then monitored.

Human breast carcinomas patients and metastatic bone lesions

Four patients with newly diagnosed breast cancer underwent neoadjuvant chemotherapy as previous described (24). Residual tumor tissues were collected at the time of surgery (which took place 21-28 days after the last dose of PTX). Biopsies of bone metastatic lesions were also obtained from 5 advanced breast cancer patients. All biopsies were obtained under informed consent following procedures approved by the Ottawa Health Sciences Research Ethics Board. Samples were collected as previously described (25). All biopsies were taken within 6-15 days of treatment with either chemotherapy alone (PTX, docetaxel or 5-fluoruracil/doxorubicin/cyclophosphamide with or without pamidronate.

Immunofluorescence and immunohistochemistry studies

Frozen tumor sections were blocked with 1% BSA and 5% goat serum for 30 minutes and incubated with various primary antibodies (**Table 1)**, for 1h at RT. Alexa Fluor-conjugated anti-rabbit or anti-rat secondary antibodies were used with unconjugated primary antibodies. For BrdU staining, DNA in frozen tissue sections was denatured with 2NHCl for 15 minutes prior to immunostaining, as described above. Nuclei in all tumor sections were counterstained with DAPI. Formalin-fixed, paraffin-embedded tissues were rehydrated, peroxidase blocked, then antigen retrieved, serum blocked and incubated with primary antibodies for 1-2h. Primary

antibodies were detected with appropriate ABC or Polymer detection kits followed by chromagen staining with DAB.

Distribution of MRC1+ TAMs relative to blood vessels in human primary breast tumors

The number of $MRC1^+$ TAMs present within a 250μm radius of a given blood vessel was counted in 6 randomly selected areas per tumor section. Then, within this 250 μm radius, the distance of each $MRC1^+$ TAM was measured to the nearest vessel and the number of $MRC1^+$ TAMs within or beyond 150 μm from that vessel was expressed as a % $MRC1^+$ TAMs within the region being analysed. These were defined as 'perivascular' or 'avascular' $MRC1^+$ TAM subsets respectively.

Tumor dissociation/flow cytometry studies

Tumors were enzymatically dissociated and labelled with antibodies as described previously (9). All antibody incubations were performed for 1h at 4^oC. Cell staining analyses and cell sorting experiments were performed using BD LSRII and BD FACSAria, respectively.

VEGFA ELISA studies

$CD45^+CD11b^+Ly6G^-F4/80^+$ TAMs were isolated from three pooled, dissociated control and CTX-treated LLC1 tumors. One hundred thousand sorted cells were seeded in 100 μL of medium and cultured overnight. Conditioned medium was examined for VEFGA release using a mouse VEGFA Quantikine Sandwich ELISA (R&D Systems).

***C*hemotaxis assay**

$MRC1^{+/Hi}$ ($CD11b^+Ly6G^-F4/80^+MRC1^{Hi}$) and $MRC1^{-/Lo}$ ($CD11b^+Ly6G^-F4/80^+MRC1^{Hi}$) TAMs were FACSorted from dissociated CTX-treated LLC1 tumours and seeded into transwell inserts (4μm pores, VWR International), $50x10^3$ cell per well. Lower chambers contained either medium

alone, medium supplemented with 10nM BSA or 10nM recombinant murine CXCL12 (100 ng/mL). Following an incubation of 6h at 37^{o}C the chambers were dissassembled and the membranes stained with crystal violet. The upper surface of each transwell insert was scraped to remove non-migrated cells before quantification.

Quantification of spontaneous LLC1 lung metastases

Sections (4μm thick) were cut from formalin-fixed paraffin-embedded lungs and stained with haemotoxylin and eosin. These stained sections were imaged using the Aperio slide scanner (Leica Biosystems), and the number of metastases per section and total metastatic area quantified using ImageScope analysis software (Leica Biosystems).

Statistics

All data represent mean values ± SEMs. *P* values of less than 0.05 were considered to be significant. All statistical comparisons were made using the non-parametric Mann-Whitney *U*-test (paired or unpaired as appropriate).

Results

M2-skewed (MRC1^{+}TIE2^{HI}VEGFA^{+}) TAMs are abundant in mouse tumors after chemotherapy and promote their relapse.

Three i.p. injections of the cytotoxic agent, cyclophosphamide (CTX), resulted in the complete cessation of LLC1 tumor growth, followed by regrowth beginning 7 days after treatment stops (**Fig. 1A, left panel**). Forty-eight hours after the last CTX injection (day 6), LLC1s contained significantly (P<0.05) shorter blood vessels and more hypoxia than size-matched controls (**Fig. S1A**). Consistent with earlier observations for MMTV-PyMT implants treated with PTX (13), TAMs were enriched among those leukocytes present in LLC1s 48h post-

CTX (**Fig. S1B**). Additionally, there was a significant (P<0.05) increase in the overall number of F4/80$^+$ TAMs in CTX-treated LLCs compared to size-matched controls. This was also seen in PTX-treated, orthotopic 4T1 tumors and doxorubicin (DOX)-treated orthotopic MMTV-PyMT implants (**Fig. S1C**).

CTX treatment of LLC1s resulted in a significant (P<0.05) increase in the number of F4/80$^+$ TAMs expressing the M2-marker, MRC1, relative to size-matched controls. In contrast, there was a significant (P<0.05) drop in F4/80$^+$/MRC1$^-$ TAMs after CTX (**Fig. 1A, right panels**). Also, TAMs from CTX-treated LLC1s expressed higher surface MRC1 than those from size-matched controls (**Fig. 1B**). Consistent with previous findings in untreated mouse tumors (9,10), MRC1^{Hi} TAMs in CTX-treated LLC1s co-expressed elevated TIE2 (**Fig. 1C&D**). A similar increase in MRC1$^+$ TAMs was also seen in orthotopic 4T1 and MMTV-PyMT implants after PTX and DOX, respectively (**Fig. S1D**). In all 3 models, the vast majority of MRC1$^+$ cells F4/80$^+$ TAMs, and the small number of F4/80$^-$MRC1$^+$ (presumably dendritic) cells were not significantly increased following treatment with CTX, PTX or DOX (**Fig. S2A**).

BrdU uptake was negligible in MRC1$^+$ TAMs in both size-matched control and CTX-treated LLC1 tumors, indicating their non-proliferative status (**Fig. S2B**). As chemotherapy-induced changes in circulating hematopoietic stem and progenitor cells (HS/PCs) could, in theory, contribute to the increase of TAM numbers post-therapy, we also performed dual immunofluorescence labelling for HS/PC markers, c-Kit and Sca1. While c-Kit$^+$Sca1$^+$ cells were detected in the spleens of LLC1 tumor-bearing mice (positive control for the staining) no such cells were detected in either control or CTX-treated LLC1s (**Fig. S2C**). These data indicate that the chemotherapy-induced increase in TAMs is most likely to be due to increased monocyte recruitment rather than the proliferation of existing TAMs or their differentiation from recruited HS/PCs.

We then isolated F4/80$^+$MRC1$^{+/Hi}$ and F4/80$^+$MRC1$^{-/Lo}$ TAMs from CTX-treated LLC1 tumors by FACS and injected them into CTX-treated LLC1 tumors in littermates (**Fig. 2A**).

MRC1$^{+/Hi}$ TAMs, but not MRC1$^{-/Lo}$ TAMs from treated tumors or TAMs from vehicle-treated tumors, accelerated tumor regrowth after CTX. This was accompanied by a significant (P<0.05) increase in the number of MRC1^{+} TAMs, CD31^{+} blood vessels and a moderate increase in BrdU^{+} (proliferating) cells in CTX-treated LLC1s receiving MRC1$^{+/Hi}$ TAMs. Very few (< 1%) of CD45+ leukocytes contained immunodetectable BrdU (**Fig. 2B-E**).

MRC1^{+} TAMs are proangiogenic in untreated tumors and express the important pro-angiogenic mediator VEGFA (9,26). Moreover, myeloid-specific deletion of VEGFA is known to have profound effects on the vascularisation and progression of untreated mouse tumors (27). We, therefore, investigated the role of VEGFA derived from MRC1^{+} TAMs in tumor-relapse after chemotherapy. As reported previously in mouse tumors (25), VEGFA was expressed by both TAMs and other (F4/80^{-}) cells in control LLC1s (**Fig. 3A & Fig. S3A**). However, within 48h of the last dose of CTX, VEGFA was expressed almost exclusively by MRC1^{+} TAMs (**Fig. S3B**). As the expression of VEGFA was closely associated with MRC1^{+} TAMs, and because the latter were more abundant in CTX-treated LLCs (**Fig. 3B&C**), we postulated that the macrophage population as a whole found within CTX-treated LLCs might be capable of producing higher levels of VEGFA. Indeed, the release of VEGFA was found to be significantly greater for TAMs sampled from CTX-treated LLCs (**Fig. 3D**).

MDSCs (CD11b^{+}Gr1^{+}) in tumour-bearing mice are also reported to express MRC1 raising the possibility that some VEGFA-expressing MRC1^{+} cells in CTX-treated tumours might have been MDSCs (28). However, we found that both granulocytic (CD45^{+}CD11b^{+}Ly6G^{+}) and monocytic (CD45^{+}CD11b^{+}Ly6G^{-}Ly6C^{+}) MDSC subsets were depleted in CTX-treated tumours, and that the expression of MRC1 on monocytic MDSCs was significantly (P<0.05) lower than that on TAMs (Fig. S3C). Taken together, these data suggest that MDSCs are unlikely to represent a significant proportion of the MRC1^{Hi} cells in our LLC1 tumors.

We previously showed that a subset of TAMs accumulate in hypoxic areas of untreated mouse and human tumors (29), where they respond to hypoxia by upregulating hypoxia-

inducible factors (HIFs) 1 and 2 and a wide array of HIF-dependent M2 genes (30). As we detected some MRC1$^+$ TAMs in the hypoxic regions of CTX-treated LLC1 tumors (**Fig. S4A**), albeit at much lower numbers than in the well-vascularised, normoxic (PIMO$^-$) regions (**Fig. 4A**), we investigated the possibility that hypoxia-regulated transcriptional programming (via HIFs 1 and 2) might contribute to the relapse-promoting functions of TAMs. LLC1s were implanted into LysM$^{Cre/+}$HIF1$^{fl/fl}$ or LysM$^{cre/+}$HIF2$^{fl/fl}$ myeloid-specific knockout mice and treated with vehicle or CTX. HIF knockout was seen to have no effect on the number of MRC1$^+$ TAMs in either the hypoxic or PIMO$^-$ areas in CTX-treated LLC1s, nor on tumor relapse (**Fig. S4B&C**). Immunohistochemical staining demonstrated a reduction of >90% in TAMs expressing HIF-1α or 2α in control LLC1s, confirming high efficiency of LysCre-targeted HIF allele ablation in our mice (**Fig. S4D**). These data suggest that hypoxia and HIF1/2-regulated transcriptional programming do not regulate the relapse-promoting functions of MRC1$^+$ TAMs.

MRC1$^+$ TAMs accumulate in well-vascularised areas of tumors after chemotherapy in both mouse and human tumors and promote tumor relapse: role of VEGFA

Previous studies have shown that MRC1$^+$ TAMs can reside close to blood vessels in untreated mouse tumors (10). Furthermore, the aforementioned HIF knockout study demonstrated an increase in MRC1$^+$ TAMs in PIMO$^-$ vascularised areas (PIMO$^-$ VA) in CTX-treated tumors (**Fig. S4B**). We, therefore, conducted a more detailed immunofluorescence staining analysis of the distribution of these cells in control and CTX-treated LLC1s. This showed that, while MRC1$^+$ TAMs were evenly distributed between PIMO$^-$ VA and PIMO$^+$ hypoxic areas in size-matched control tumors, there was a significant (P<0.05) increase in the number of F4/80$^+$MRC1$^+$TAMs in the former in CTX-treated LLC1s (**Fig. 4A**). As CTX treatment also resulted in reduced tumor vascularity (**Fig. S1A**) we normalized MRC1$^+$ TAM numbers to CD31$^+$ area in PIMO$^-$ VA of control and CTX-treated LLC1s. Interestingly, this showed that the increase in MRC1$^+$ TAMs in

PIMO$^-$ VA is independent of changes in the vasculature (**Fig. 4A, far right panel**). Further immunofluorescent analysis of 4T1 and PyMT-MMTV tumors demonstrated a similar increase in the number of vessel-associated MRC1$^+$ TAMs after treatment with PTX and DOX, respectively (**Fig. 4B**). Furthermore, because the majority of MRC1$^+$ TAMs co-expressed VEGFA in both control and CTX-treated LLCs this meant that there was also a significant increase in VEGFA$^+$ TAMs in perivascular areas (**Fig. 4C** upper panel). Interestingly, there was also a significant (P<0.05) increase in the number of MRC1$^+$VEGFA$^+$ TAMs in direct contact with the abluminal surface of the tumor vasculature in CTX-treated tumors (**Fig. 4C** lower panel). However, the preferential accumulation of MRC1$^+$VEGFA$^+$ TAMs in the PIMO–VA regions of chemotherapy-treated tumors was no longer present following relapse, suggesting that the accumulation of MRC1$^+$ TAMs was an acute, transient response to therapy (**Fig. S5A**). MRC1$^+$ TAMs were also seen to preferentially localize in perivascular areas (ie. within 150μm of blood vessels) in human breast carcinomas 21-28 days after 3 cycles of neoadjuvant PTX (**Fig. 4D** left and middle panels), and in breast cancer metastases in the bone after chemotherapy (with or without bisphosphonates) (**Fig. 4D** right panel).

Immunofluorescence staining of VEGFA in orthotopic MMTV-PyMT tumors excised at day 6 indicated that only MRC1$^+$, not MRC1$^-$, TAMs expressed detectable levels of VEGFA in vehicle and DOX-injected Cre$^-$ tumors. Indeed, >98% of vessel-associated MRC1$^+$ TAMs were VEGFA$^+$ in both groups of tumors (**Fig. 5A&B**). So, we investigated the role of VEGFA expression by these MRC1$^+$ TAMs in tumor relapse using the *Csf1r*-Mer-Cre-Mer inducible cre-recombinase/estrogen receptor fusion protein model for the tamoxifen-induced ablation of VEGFA selectively in monocytes/macrophages (23).

Female *Csf1r-Mer-iCre-Mer* FVB/n mice were orthotopically implanted with syngeneic MMTV-PyMT tumors and administered tamoxifen 24h after a single injection of either vehicle or DOX. In addition, tamoxifen was given continuously thereafter to ensure VEGFA knockout until mice were sacrificed at the end of the experiment (day 14), with the same treatment given to

control Cre-recombinase negative mice (**Fig. 5C**). As the implanted PyMT cells in these tumors did not carry the *Csf1r*-driven Cre recombinase and expression of *Csf1r* is largely confined to TAMs in such tumors, the knockdown of VEGFA was restricted to the macrophage lineage, a significant source of VEGFA in the PyMT model (31) (as in CTX-treated LLC1s). Tamoxifen-induced ablation of this TAM-derived VEGFA (**Fig. 5C**) caused a significant (P<0.05) delay in the growth of vehicle-treated MMTV-PyMT tumors (**Fig. 5D**). Furthermore, relapse of DOX-treated tumors lacking VEGFA$^+$ TAMs (Cre$^+$) was significantly (P<0.05) slower than that of DOX-treated tumors in VEGFA-expressing (Cre$^-$) mice (**Fig. 5E**). This was accompanied by a significant (P<0.05) decrease in vessel area in these tumors (**Fig. 5F**).

Pharmacological blockade of CXCR4 prevents perivascular accumulation of MRC1$^+$ VEGFA$^+$ TAMs after chemotherapy and delays tumor relapse.

The majority of F4/80$^+$MRC1$^+$ TAMs expressed the CXCL12 receptor, CXCR4 in both control and CTX-treated LLC1s (**Fig. 6A**) and 98% of all CXCR4-expressing cells were TAMs in CTX-treated LLC1 tumors, compared to 78% in control LLCs (where other cell types were also CXCR4$^+$) (**Fig. 6B**). As reported previously (32,33), LLC1 cells do not express CXCR4 (**Fig. 6A-B**). Moreover, less than 1% of CD31+ blood vessels expressed CXCR4 in CTX-treated tumors (**Fig. 6C**). MRC1^{Hi} TAMs in both control and CTX-treated tumors expressed elevated levels of CXCR4 compared with the MRC1^{Lo} TAMs (**Figure 6D**).

These changes in CXCR4$^+$ cells after CTX were accompanied by a marked increase in tumor levels of its ligand, CXCL12, on day 6 (**Fig. 6D, far right)**. These CXCL12$^+$ cells were CD31$^-$ (**Fig. 6E**, **left panel**) and most likely tumor cells and/or fibroblasts (34). As a hypoxia-inducible gene (35), it was not surprising to find CXCL12 more highly expressed in hypoxic than normoxic areas of control LLC1 tumors. However, after CTX, tumor levels of HIFs-1 and 2 were markedly reduced in all areas of tumors (**Fig. S6A, i and ii**) but CXCL12 was abundant in both

hypoxic and normoxic, vascularised areas (**Fig. S6B**). This suggested CXCL12 upregulation by factors other than hypoxia in such tumors.

CTX is known to induce oxidative stress (36), a cellular response known to regulate the expression of CXCL12 (37), so we investigated the expression of a well-defined marker for oxidative stress, hemeoxygenase-1 (HMOX-1) in control vs CTX-treated tumors. Interestingly, this was found to be upregulated in perivascular, $PIMO^-$, CXCL12-rich areas of tumors after CTX treatment but not in control tumors (**Fig. S6C, i and ii)**. Both $MRC1^+$ TAMs and $MRC1^-$ cells expressed HMOX-1 in these vascularised areas (**Fig. S6C iii)**.

We then investigated whether CXCL12 might recruit and/or retain $CXCR4^+MRC1^+$ TAMs in LLC1 tumors. First, we showed in an *in vitro* chemotaxis assay that CXCL12 is selectively chemotactic for $MRC1^{+/Hi}$ TAMs isolated from LLC1 tumors (**Fig. 6E, right panel**). Then we administered CTX to LLC1-bearing mice alone or in combination with the CXCR4 antagonist, plerixafor (AMD3100) (**Fig 7A**). This was feasible as TAMs were the predominant cell type expressing CXCR4 after CTX (**Fig. 6B**). CXCR4 blockade significantly inhibited CTX-induced accumulation of $F4/80^+$ $MRC1^+$ TAMs in the $PIMO^-$ VA (while the numbers in $PIMO^+$ areas of LLC1 tumors were unchanged, as was $F4/80^+$ $MRC1^-$ TAMs in either of these areas) and delayed tumor relapse (**Figs. 7A&B and S5B)**. At day 10 (when tumors had relapsed in the CTX alone group), a similar distribution of $MRC1^+$ TAMs was seen compared to day 6 (the start of the relapse period) (**Fig. 7B&C**). In addition, tumors administered CTX+AMD3100 contained significantly ($P<0.05$) shorter $CD31^+$ blood vessels, higher levels of hypoxia and fewer $BrdU^+$ (proliferating) cells than tumors exposed to CTX with the vehicle for AMD3100 (PBS) (**Fig. 7D & Fig. S5C**).

We then examined the effect of CXCR4 blockade on the distribution of $MRC1^+$ TAMs across $PIMO^-$ VAs in CTX-treated tumors. Interestingly, this was found to significantly ($P<0.05$) reduce the number of $MRC1^+$ TAMs in direct contact with the abluminal surface of CD31+ blood vessels (standardised by CD31+ vessel area as this differed between CTX+PBS and CTX+

AMD3100 groups), and increase them elsewhere in the $PIMO^-$ VAs (**Figure 7E**). These data suggest that CXCR4 regulates the direct association of alternatively activated TAMs with blood vessels in CTX-treated LLC1s.

A recent study demonstrated a marked rebound in the growth of pulmonary metastases after treatment with an antibody to CCL2 (38). This was the result of increased mobilization of monocytes from the bone marrow after CCL2 inhibition, and increased blood vessel formation and cancer cell proliferation in the lungs. We, therefore, investigated the possibility of a similar rebound effect after CXCR4 inhibition using AMD3100 as this could disrupt the bone marrow niche. When we extended the length of the AMD3100 experiment, primary LLC1 tumors relapsed eventually, but not at an accelerated rate, and mice receiving CTX+AMD3100 showed increased survival compared to those in the CTX alone group (or controls). Importantly, there was also no rebound in pulmonary metastases (**Fig. S8)**.

Discussion

Our studies show that M2-skewed TAMs ($MRC1^+TIE2^+CXCR4^{Hi}VEGFA^+$) selectively accumulate in vascularized, well-oxygenated areas of LLC1 tumors after treatment with CTX. A similar increase in such vessel-associated, M2-skewed TAMs was also seen in orthotopic 4T1 and MMTV-PyMT implants after treatment with PTX and DOX, respectively, and in human breast carcinomas following neoadjuvant treatment with PTX. This perivascular accumulation was found to be CXCR4-dependent, especially the increased, direct contact of this TAM subset with the abluminal surface of blood vessels in chemotherapy-treated tumors. When this was disrupted using a CXCR4 inhibitor, tumor revascularisation and regrowth after chemotherapy were markedly impaired. We also show, using an inducible, macrophage-specific, gene knockdown model that VEGFA expressed by such $MRC1^+$ TAMs mediates, in part, their ability

to promote tumor relapse after therapy. Consistent with this, genetic deletion of HIF signaling in TAMs in hypoxic tumor areas had no effect on this.

The mobilisation, and accumulation in tumors, of such BMDCs as myelomonocytic cells, MDSCs, endothelial progenitor cells (EPCs) and macrophages after various forms of anti-cancer therapy is now well-established (13-19,39,40). However, our data show that M2-skewed TAMs represent a significant proportion of such BMDCs in tumors after chemotherapy, and is not accompanied by TAM proliferation or increased numbers of stem/progenitor cells. These data suggest that increased recruitment of circulating monocytes precedes the accumulation of such M2 TAMs in tumors after chemotherapy. It remains to be seen whether monocytes are already M2-skewed upon arrival in treated tumors and/or activated by factors produced in the perivascular niche. Of note, the recruitment, activation and perivascular retention of these cells does not appear to be just an acute response to chemotherapy-induced tumor damage, as increased numbers of perivascular M2 TAMs persisted throughout the relapse phase.

Our observations suggest that the accumulation of $MRC1^{+}VEGFA^{+}$ TAMs on and around the tumor vasculature plays an important part in tumor revascularisation and relapse after chemotherapy. Furthermore, this was accompanied by a marked change in the pattern of CXCL12 expression in tumors. While CXCL12 was mainly confined to hypoxic areas of control tumors, it was upregulated in vascularised, well oxygenated areas after chemotherapy. This correlated with an increase in the expression of the enzyme, HMOX-1, a marker of oxidative stress, in such perivascular areas. Cytotoxic agents like CTX induce oxidative stress in tumors (41) which activates cellular expression of HMOX-1. This, in turn, generates carbon monoxide from the breakdown of heme - a gas known to upregulate both CXCL12 and VEGFA in neighbouring cells (37). Interestingly, HMOX-1 also regulates expression of MRC1 by macrophages (42). So, chemotherapy-induction of this stress pathway in perivascular areas could both retain TAMs via local CXCL12 induction, and upregulate their expression of VEGFA

and MRC1. Interestingly, the CXCL12-induced retention of myeloid cells around the vasculature is also essential to the process of neovascularization in non-malignant tissues (43).

Other factors may also contribute to the retention of $MRC1^+$ TAMs. Our observation that $MRC1^+$ TAMs expressed elevated TIE2 suggests that ANGPT2 expressed by the tumor endothelium (44) might also be involved. Indeed, ANGPT2 has an established role in retaining vascular modulatory myeloid cells in proximity to the vasculature in progressing mouse tumors (26).

In untreated mouse tumors, perivascular, M2-skewed TAMs have an established vascular modulatory role and facilitate tumor growth and progression (26). Our observation that chemotherapy induces the accumulation of $MRC1^+VEGFA^+$ TAMs around tumor blood vessels strongly infers a proangiogenic role for these cells. This is supported by our finding that pharmacological inhibition of their chemotherapy-induced accumulation resulted in reduced subsequent tumor revascularisation. Furthermore, in DOX-treated, MMTV-PyMT tumor implants VEGFA was found to be expressed predominantly by $MRC1^+$ TAMs, consistent with our previous finding that TAMs are a major source of VEGFA in MMTV-PyMT tumors (31). The selective ablation of VEGFA in $MRC1^+$ TAMs resulted in delayed tumor relapse, post-therapy. However, PyMT tumors still relapsed, albeit at a reduced rate, in the absence of TAM-derived VEGFA, indicating that other TAM-derived factors may also contribute to tumor relapse and/or the possible induction of resistance mechanisms in tumors to VEGFA knockout. The presence of the latter has been demonstrated in tumors after anti-VEGFA therapy and shown to include increased expression of such alternative pro-angiogenic mediators as FGF2 (45), ANGPT2 (46) or PlGF (47) and the recruitment of tumor-promoting, $CD11b^+$ $Gr1^+$ myeloid cells (48).

Recently, the Condeelis group have used intravital imaging to characterise a distinct subset of perivascular TAMs in untreated mouse tumors that make contact with endothelial cells and tumor cells expressing high levels of Mena (a protein that enhances their motility), and directly stimulate tumor cell intravasation (49). These cell trios have been termed 'Tumor

Microenvironments of Metastasis' (TMEMs). It is possible that some of the perivascular MRC1+ M2-skewed TAMs accumulating around tumor blood vessels after chemotherapy form TMEMs and promote metastasis as well as relapse – a dangerous combination in patients with inoperable tumors.

The effect of CXCR4 blockade on tumor relapse after chemotherapy in our study suggests that CXCR4 inhibitors might be successfully combined with chemotherapy. This combination could extend relapse-free survival in patients with inoperable tumors, although our data suggests that multiple rounds of the inhibitor would have to be administered to maintain a suppressive effect on relapse. Such sustained use of a CXCR4 antagonist after chemotherapy could conceivably disrupt the marrow niche. However, this is unlikely to lead to clinical problems as a recent, first-in-human clinical trial has shown that repeated daily injections of the CXCR4 antagonist, LY2510924 over a number of consecutive, 28-day cycles was well tolerated in advanced cancer patients (50).

Taken together, our data suggest that the selective targeting of relapse-promoting, perivascular TAMs could delay the relapse of both primary and metastatic tumors in patients after chemotherapy, thereby extending their relapse-free survival.

Acknowledgments

This study was supported mainly by a Cancer Research UK grant to CEL. She also gratefully acknowledges the support of Yorkshire Cancer Research. Other authors acknowledge the grant support of the Swiss Cancer League (to MDP), Breast Cancer Research Foundation (to OCO & JAJ), a Chancellor's Fellowship from the University of Edinburgh (to B-ZQ), and The Wellcome Trust (Senior Investigator Award) to JWP.

References

1. Savir G, Huber KE, Saif MW. Locally advanced pancreatic cancer. Looking beyond traditional chemotherapy and radiation. JOP : Journal of the pancreas 2013;14(4):337-9.
2. Strom HH, Bremnes RM, Sundstrom SH, Helbekkmo N, Aasebo U. Poor prognosis patients with inoperable locally advanced NSCLC and large tumors benefit from palliative chemoradiotherapy: a subset analysis from a randomized clinical phase III trial. Journal of thoracic oncology : official publication of the International Association for the Study of Lung Cancer 2014;9(6):825-33.
3. Coffelt SB, Lewis CE, Naldini L, Brown JM, Ferrara N, De Palma M. Elusive identities and overlapping phenotypes of proangiogenic myeloid cells in tumors. Am J Pathol 2010;176(4):1564-76.
4. Noy R, Pollard JW. Tumor-Associated Macrophages: From Mechanisms to Therapy. Immunity 2014;41(1):49-61.
5. Qian BZ, Pollard JW. Macrophage diversity enhances tumor progression and metastasis. Cell 2010;141(1):39-51.
6. Movahedi K, Laoui D, Gysemans C, Baeten M, Stange G, Van den Bossche J, et al. Different tumor microenvironments contain functionally distinct subsets of macrophages derived from Ly6C(high) monocytes. Cancer Res 2010;70(14):5728-39.
7. Coffelt SB, Hughes R, Lewis CE. Tumor-associated macrophages: effectors of angiogenesis and tumor progression. Biochimica et biophysica acta 2009;1796(1):11-8.
8. Biswas SK, Sica A, Lewis CE. Plasticity of macrophage function during tumor progression: regulation by distinct molecular mechanisms. Journal of immunology 2008;180(4):2011-7.
9. Pucci F, Venneri MA, Biziato D, Nonis A, Moi D, Sica A, et al. A distinguishing gene signature shared by tumor-infiltrating Tie2-expressing monocytes, blood "resident"

monocytes, and embryonic macrophages suggests common functions and developmental relationships. Blood 2009;114(4):901-14.

10. De Palma M, Venneri MA, Galli R, Sergi Sergi L, Politi LS, Sampaolesi M, et al. Tie2 identifies a hematopoietic lineage of proangiogenic monocytes required for tumor vessel formation and a mesenchymal population of pericyte progenitors. Cancer Cell 2005;8(3):211-26.
11. Daenen LG, Houthuijzen JM, Cirkel GA, Roodhart JM, Shaked Y, Voest EE. Treatment-induced host-mediated mechanisms reducing the efficacy of antitumor therapies. Oncogene 2014;33(11):1341-7.
12. De Palma M, Lewis CE. Macrophage regulation of tumor responses to anticancer therapies. Cancer Cell 2013;23(3):277-86.
13. DeNardo DG, Brennan DJ, Rexhepaj E, Ruffell B, Shiao SL, Madden SF, et al. Leukocyte complexity predicts breast cancer survival and functionally regulates response to chemotherapy. Cancer Discov 2011;1(1):54-67.
14. Nakasone ES, Askautrud HA, Kees T, Park JH, Plaks V, Ewald AJ, et al. Imaging tumor-stroma interactions during chemotherapy reveals contributions of the microenvironment to resistance. Cancer Cell 2012;21(4):488-503.
15. Shree T, Olson OC, Elie BT, Kester JC, Garfall AL, Simpson K, et al. Macrophages and cathepsin proteases blunt chemotherapeutic response in breast cancer. Genes Dev 2011;25(23):2465-79.
16. Ahn GO, Tseng D, Liao CH, Dorie MJ, Czechowicz A, Brown JM. Inhibition of Mac-1 (CD11b/CD18) enhances tumor response to radiation by reducing myeloid cell recruitment. Proc Natl Acad Sci U S A 2010;107(18):8363-8.
17. Kioi M, Vogel H, Schultz G, Hoffman RM, Harsh GR, Brown JM. Inhibition of vasculogenesis, but not angiogenesis, prevents the recurrence of glioblastoma after irradiation in mice. J Clin Invest 2010;120(3):694-705.

18. Kozin SV, Kamoun WS, Huang Y, Dawson MR, Jain RK, Duda DG. Recruitment of myeloid but not endothelial precursor cells facilitates tumor regrowth after local irradiation. Cancer Res 2010;70(14):5679-85.

19. Welford AF, Biziato D, Coffelt SB, Nucera S, Fisher M, Pucci F, et al. TIE2-expressing macrophages limit the therapeutic efficacy of the vascular-disrupting agent combretastatin A4 phosphate in mice. J Clin Invest 2011;121(5):1969-73.

20. Mantovani A, Biswas SK, Galdiero MR, Sica A, Locati M. Macrophage plasticity and polarization in tissue repair and remodelling. The Journal of pathology 2013;229(2):176-85.

21. Browder T, Butterfield CE, Kraling BM, Shi B, Marshall B, O'Reilly MS, et al. Antiangiogenic scheduling of chemotherapy improves efficacy against experimental drug-resistant cancer. Cancer Res 2000;60(7):1878-86.

22. Affara NI, Ruffell B, Medler TR, Gunderson AJ, Johansson M, Bornstein S, et al. B cells regulate macrophage phenotype and response to chemotherapy in squamous carcinomas. Cancer Cell 2014;25(6):809-21.

23. Qian BZ, Li J, Zhang H, Kitamura T, Zhang J, Campion LR, et al. CCL2 recruits inflammatory monocytes to facilitate breast-tumour metastasis. Nature 2011;475(7355):222-5.

24. Wyckoff JB, Wang Y, Lin EY, Li JF, Goswami S, Stanley ER, et al. Direct visualization of macrophage-assisted tumor cell intravasation in mammary tumors. Cancer Res 2007;67(6):2649-56.

25. Hilton JF, Amir E, Hopkins S, Nabavi M, DiPrimio G, Sheikh A, et al. Acquisition of metastatic tissue from patients with bone metastases from breast cancer. Breast cancer research and treatment 2011;129(3):761-5.

26. Mazzieri R, Pucci F, Moi D, Zonari E, Ranghetti A, Berti A, et al. Targeting the ANG2/TIE2 axis inhibits tumor growth and metastasis by impairing angiogenesis and disabling rebounds of proangiogenic myeloid cells. Cancer Cell 2011;19(4):512-26.

27. Stockmann C, Doedens A, Weidemann A, Zhang N, Takeda N, Greenberg JI, et al. Deletion of vascular endothelial growth factor in myeloid cells accelerates tumorigenesis. Nature 2008;456(7223):814-8.

28. Kodumudi KN, Woan K, Gilvary DL, Sahakian E, Wei S, Djeu JY. A novel chemoimmunomodulating property of docetaxel: suppression of myeloid-derived suppressor cells in tumor bearers. Clin Cancer Res 2010;16(18):4583-94.

29. Murdoch C, Giannoudis A, Lewis CE. Mechanisms regulating the recruitment of macrophages into hypoxic areas of tumors and other ischemic tissues. Blood 2004;104(8):2224-34.

30. Fang HY, Hughes R, Murdoch C, Coffelt SB, Biswas SK, Harris AL, et al. Hypoxia-inducible factors 1 and 2 are important transcriptional effectors in primary macrophages experiencing hypoxia. Blood 2009;114(4):844-59.

31. Lin EY, Li JF, Gnatovskiy L, Deng Y, Zhu L, Grzesik DA, et al. Macrophages regulate the angiogenic switch in a mouse model of breast cancer. Cancer Res 2006;66(23):11238-46.

32. Miao Z, Luker KE, Summers BC, Berahovich R, Bhojani MS, Rehemtulla A, et al. CXCR7 (RDC1) promotes breast and lung tumor growth in vivo and is expressed on tumor-associated vasculature. Proc Natl Acad Sci U S A 2007;104(40):15735-40.

33. Weiss ID, Jacobson O, Kiesewetter DO, Jacobus JP, Szajek LP, Chen X, et al. Positron emission tomography imaging of tumors expressing the human chemokine receptor CXCR4 in mice with the use of 64Cu-AMD3100. Molecular imaging and biology : MIB : the official publication of the Academy of Molecular Imaging 2012;14(1):106-14.

34. Feig C, Jones JO, Kraman M, Wells RJ, Deonarine A, Chan DS, et al. Targeting CXCL12 from FAP-expressing carcinoma-associated fibroblasts synergizes with anti-PD-L1 immunotherapy in pancreatic cancer. Proc Natl Acad Sci U S A 2013;110(50):20212-7.

35. Hitchon C, Wong K, Ma G, Reed J, Lyttle D, El-Gabalawy H. Hypoxia-induced production of stromal cell-derived factor 1 (CXCL12) and vascular endothelial growth factor by synovial fibroblasts. Arthritis and rheumatism 2002;46(10):2587-97.

36. Li L, Jiang L, Geng C, Cao J, Zhong L. The role of oxidative stress in acrolein-induced DNA damage in HepG2 cells. Free radical research 2008;42(4):354-61.

37. Lin HH, Chen YH, Chang PF, Lee YT, Yet SF, Chau LY. Heme oxygenase-1 promotes neovascularization in ischemic heart by coinduction of VEGF and SDF-1. Journal of molecular and cellular cardiology 2008;45(1):44-55.

38. Bonapace L, Coissieux MM, Wyckoff J, Mertz KD, Varga Z, Junt T, et al. Cessation of CCL2 inhibition accelerates breast cancer metastasis by promoting angiogenesis. Nature 2014;515(7525):130-3.

39. Diaz-Montero CM, Salem ML, Nishimura MI, Garrett-Mayer E, Cole DJ, Montero AJ. Increased circulating myeloid-derived suppressor cells correlate with clinical cancer stage, metastatic tumor burden, and doxorubicin-cyclophosphamide chemotherapy. Cancer Immunol Immunother 2009;58(1):49-59.

40. Shaked Y, Henke E, Roodhart JM, Mancuso P, Langenberg MH, Colleoni M, et al. Rapid chemotherapy-induced acute endothelial progenitor cell mobilization: implications for antiangiogenic drugs as chemosensitizing agents. Cancer Cell 2008;14(3):263-73.

41. Chen Y, Jungsuwadee P, Vore M, Butterfield DA, St Clair DK. Collateral damage in cancer chemotherapy: oxidative stress in nontargeted tissues. Molecular interventions 2007;7(3):147-56.

42. Tu TH, Joe Y, Choi HS, Chung HT, Yu R. Induction of heme oxygenase-1 with hemin reduces obesity-induced adipose tissue inflammation via adipose macrophage phenotype switching. Mediators of inflammation 2014;2014:290708.

43. Grunewald M, Avraham I, Dor Y, Bachar-Lustig E, Itin A, Jung S, et al. VEGF-induced adult neovascularization: recruitment, retention, and role of accessory cells. Cell 2006;124(1):175-89.

44. Stratmann A, Risau W, Plate KH. Cell type-specific expression of angiopoietin-1 and angiopoietin-2 suggests a role in glioblastoma angiogenesis. Am J Pathol 1998;153(5):1459-66.

45. Casanovas O, Hicklin DJ, Bergers G, Hanahan D. Drug resistance by evasion of antiangiogenic targeting of VEGF signaling in late-stage pancreatic islet tumors. Cancer Cell 2005;8(4):299-309.

46. Rigamonti N KE, Keklikoglou I, Rmili CW, Leow CC, De Palma M. Role of angiopoietin-2 in adaptive tumor resistance to VEGF signalling blockade. Cell Reports 2014;Cell Reports (July 31, 2014).

47. Fischer C, Jonckx B, Mazzone M, Zacchigna S, Loges S, Pattarini L, et al. Anti-PlGF inhibits growth of VEGF(R)-inhibitor-resistant tumors without affecting healthy vessels. Cell 2007;131(3):463-75.

48. Shojaei F, Wu X, Malik AK, Zhong C, Baldwin ME, Schanz S, et al. Tumor refractoriness to anti-VEGF treatment is mediated by CD11b+Gr1+ myeloid cells. Nat Biotechnol 2007;25(8):911-20.

49. Roussos ET, Goswami S, Balsamo M, Wang Y, Stobezki R, Adler E, et al. Mena invasive (Mena(INV)) and Mena11a isoforms play distinct roles in breast cancer cell cohesion and association with TMEM. Clinical & experimental metastasis 2011;28(6):515-27.

50. Galsky MD, Vogelzang NJ, Conkling P, Raddad E, Polzer J, Roberson S, et al. A Phase I Trial of LY2510924, a CXCR4 Peptide Antagonist, in Patients with Advanced Cancer. Clin Cancer Res 2014;20(13):3581-8.

Figure Legends

Figure 1. Effects of cyclophosphamide (CTX) on tumor growth and accumulation of M2 TAMs in LLC1 tumors. (**A**) Growth kinetics of LLC1s following three i.p. injections with either 150 mg/kg CTX or PBS (*left*), the number of $MRC1^+$ or $MRC1^-$ $F4/80^+$ TAMs (*right*) (n=7-8/group), and (**B**) their cell-surface expression of MRC1, as detected by flow cytometry (n=5-6/group), two days after the last dose of CTX (day 6, ie prior to the regrowth phase). (**C**) Flow cytometric analysis of TIE2 and MRC1 on TAMs from CTX-treated tumors. (**D**) Co-localization of MRC1 and TIE2 on TAMs in CTX-treated tumors (see yellow arrows and inset for dual-stained cells). V = vessel. Bars=50 μm. *P<0.05.

Figure 2. Effects of adoptive transfer of $MRC1^{Hi}$ vs $MRC1^{Lo}$ TAMs on LLC1 relapse after CTX. (**A**) Design schematic of the TAM transfer experiment. (**B**) Quantification of $MRC1^+$ TAMs in tumors receiving adoptive transfer of $MRC1^{-/Lo}$ or $MRC1^{+/Hi}$ TAMs. (**C**) LLC1 regrowth after the last CTX injection ('day 0'). (**D**) Vascularisation and (**E**) proliferation in LLC1 tumors receiving $MRC1^{Hi}$ or $MRC1^{Lo}$ (n = 5/group). Co-staining of CTX-treated LLC1 tumor sections with antibodies against the pan-leukocyte marker (CD45) and BrdU. Fewer than 1% of proliferating cells were leukocytes in either group. *P<0.05. Bars=50 μm.

Figure 3. Effect of CTX on the number of $MRC1^+$ $VEGFA^+$ TAMs in LLC1 tumors and VEGFA release by TAMs *in vitro*. (A) Representative immunostaining for $F4/80^+$, $MRC1^+$ and $VEGFA^+$. VEGF-expressing $F4/80^-$ cells (*yellow arrows*) and $F4/80^+$ TAMs (*orange arrows*). (**B**) VEGFA co-localization with MRC1 in TAMs. Bar=50 μm. (**C**) Number of $MRC1^+$ $VEGFA^+$ TAMs. (**D**) VEGFA release by $CD45^+CD11b^+Ly6G^-F4/80^+$ TAMs (VEGFA release in medium over 16h, standardised by live TAM numbers) *P<0.05.

Figure 4. Effect of cytotoxic drugs on the distribution of MRC1$^+$ TAMs in mouse and human tumors: co-localization with VEGFA. (**A**) Immunostaining of MRC1$^+$ TAMs in PIMO$^-$VA and hypoxic (PIMO$^+$) areas of LLC1 tumors, 48h after last injection of CTX (left and middle), and their abundance in PIMO$^-$ VA areas normalised by CD31$^+$ area (*right*) (n=4/group). (**B**) MRC1$^+$ TAM accumulation in vessel-associated ('VA') areas in 4T1 (n=8-9/group) and MMTV-PyMT tumor implants after treatment with PTX or DOX respectively (n=7/group). (**C**) Overall number of MRC1$^+$VEGFA$^+$ TAMs in PIMO$^-$ VA (*upper*) and the number in direct contact with CD31+ vessels ('abluminal'; *lower panel*) in control and CTX-treated LLCs 48h after the final dose of CTX (both normalized by total CD31$^+$ area). (**D**) MRC1$^+$ TAMs in vascular or avascular areas of human primary carcinomas three weeks after three cycles of PTX treatment (black arrows; n=4 biopsies). MRC1$^+$ macrophages near vessels in bone metastases from patients with advanced breast cancer following treatment (red arrows; n=4 biopsies). Bars=50μm. *P<0.05.

Figure 5. Effect of TAM-derived VEGFA on relapse of orthotopic MMTV-PyMT tumors after DOX treatment. **(A)** Representative immunostaining for VEGFA in MRC1$^+$ TAMs in vascularised (CD31$^+$) areas of DOX-treated, Cre$^-$, MMTV-PyMT tumors. This was not seen for MRC1$^-$ TAMs anywhere in the same tumors **(B). (C)** Female Tg(*Csf1r-Mer-iCre-Mer)$_{1jwp}$;Vegfa$^{fl/fl}$) mice* bearing MMTV-PyMT tumors were administered tamoxifen for 24h to delete VEGFA expression in TAMs (pictures, right) after a single injection of either vehicle alone or DOX. (**D**) Growth of tumors treated with vehicle alone in Cre$^+$ and Cre$^-$ mice (n=3-6/group) and (**E**) regrowth of tumors in Cre$^+$ and Cre$^-$ mice after treatment with DOX (n=3-4/group). (**F**) CD31 staining of vessels in tumors in Cre$^-$ or Cre$^+$ mice given Dox. Bars=50μm. *P<0.05 w.r.t. tumors at the same time point in the respective Cre$^-$ group. $^+$P<0.05.

Figure 6. Expression of CXCR4 by MRC1$^+$ TAMs and upregulation of CXCLl2 in LLC1 tumors following CTX treatment. (**A**) Immunostaining of F4/80 and CXCR4, and (**B**) the % of CXCR4$^+$ cells co-expressing F4/80 in control and CTX-treated LLCs (n=4/group). (**C**) Immunostaining of CXCR4 and CD31 in CTX-treated LLCs. (**D**) Flow cytometric analysis of TAM expression of CXCR4 and MRC1 in dispersed CTX-treated LLCs (left panel), CXCR4 MFI on MRC1$^+$ vs. MRC1$^-$ TAMs (middle panel) (n=4-5/group), and tumor levels of immunodetectable CXCL12 protein in control and CTX-treated tumors (n=4/group) (right panel). **(E)** CXCL12$^+$ cells were perivascular in CTX-treated LLC1s (left panel) and exogenous rec human CXCL12 was chemotactic for MRC1$^{+/Hi}$ (but not MRC$^{-/Lo}$) TAMs isolated from LLC1 tumors. Bars=50 μm. *P<0.05.

Figure 7. Effect of the CXCR4 inhibitor, AMD3100 on LLC1 relapse after CTX: role of perivascular MRC1$^+$CXCR4^{Hi} TAMs. (**A**) Regrowth of tumors in mice treated with PBS, PBS+AMD3100, CTX+PBS, or CTX+AMD3100 (n=5-9/group). (**B**) F4/80$^+$MRC1$^+$ TAMs in the PIMO$^-$ VA and hypoxic (PIMO$^+$) areas of CTX+PBS or CTX+AMD3100 treated tumors (n=4-6/group) at days 6 and (**C**) day 10 (n=7-9/group). (**D**) Total CD31$^+$ vessel area in tumors treated with CTX+PBS and CTX+AMD3100 (at day 6 in panel A). (**E**) MRC1$^+$ TAMs in direct contact (‘abluminal) or not in contact with (‘non-abluminal’) with CD31$^+$ endothelial cells in PIMO$^-$ VA areas of either CTX+PBS or CTX+AMD3100 treated LLCs (normalised to total CD31$^+$ area in each FOV). *P<0.05.

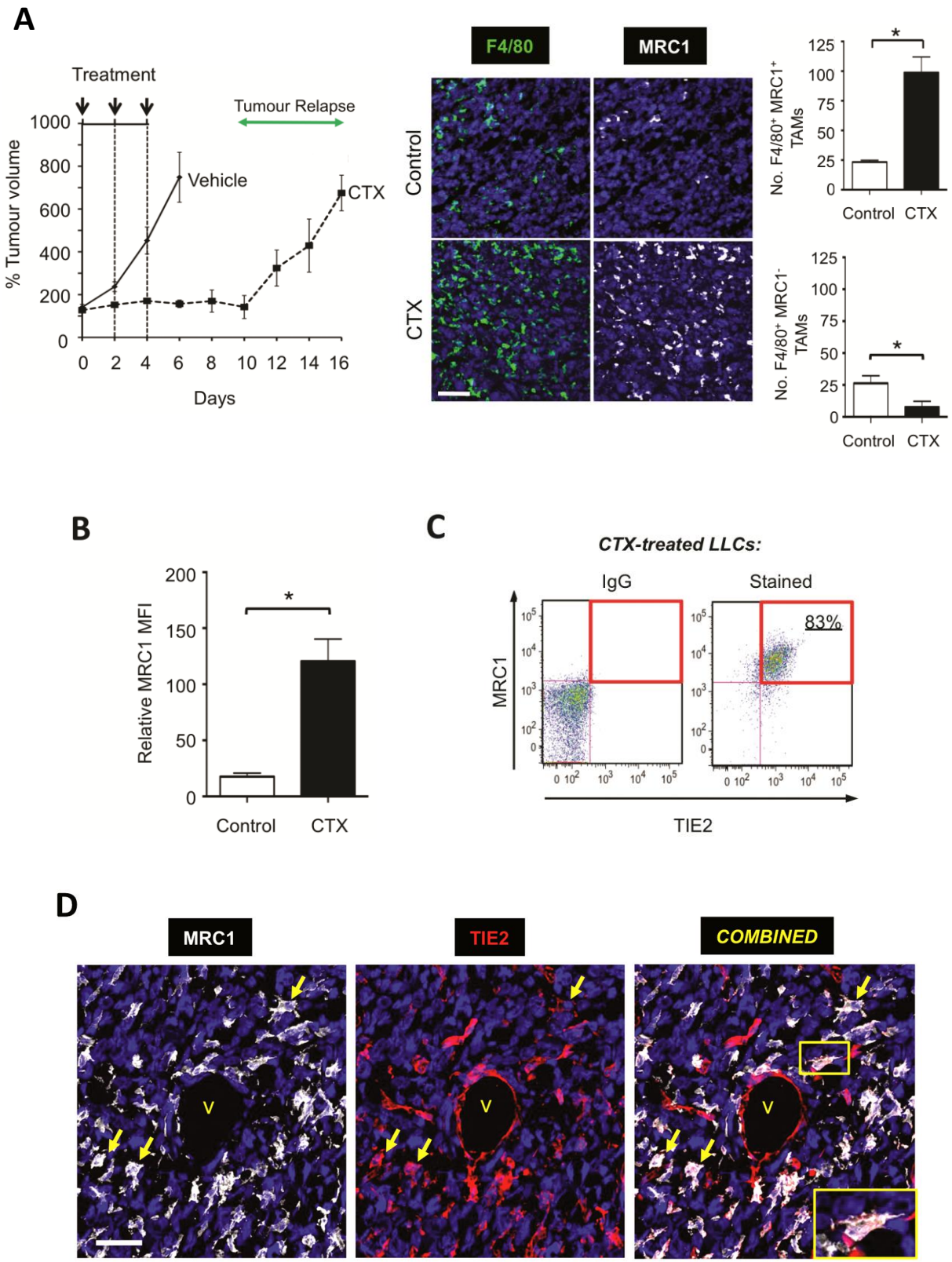
A
Treatment
Tumour Relapse
% Tumour volume
1000
800
600
400
200
0
Vehicle
CTX
0 2 4 6 8 10 12 14 16
Days
F4/80
MRC1
Control
CTX
No. F4/80+ MRC1+ TAMs
125
100
75
50
25
0
Control CTX
No. F4/80+ MRC1- TAMs
125
100
75
50
25
0
Control CTX
B
Relative MRC1 MFI
200
150
100
50
0
Control CTX
C
CTX-treated LLCs:
IgG
Stained
83%
MRC1
TIE2
D
MRC1
TIE2
COMBINED
V
V
V

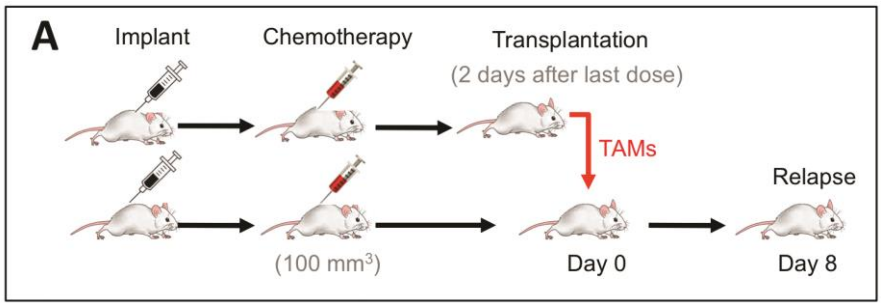
A
Implant
Chemotherapy
Transplantation
(2 days after last dose)
TAMs
Relapse
(100 mm3)
Day 0
Day 8

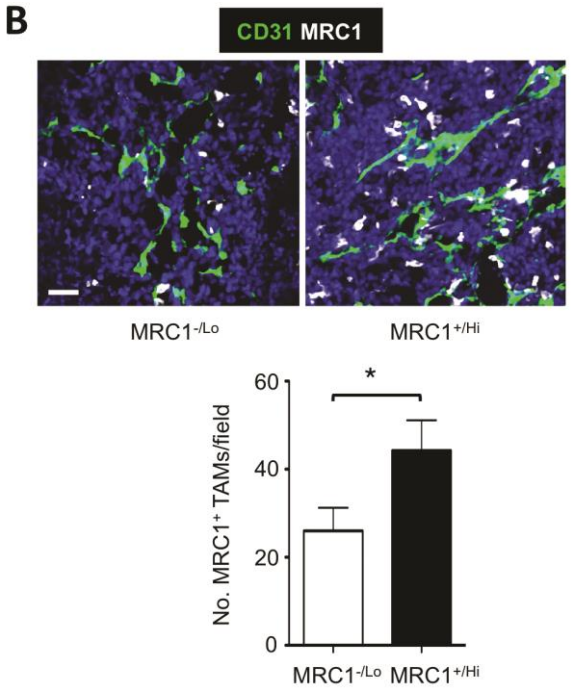
B
CD31 MRC1
MRC1-/Lo
MRC1+/Hi
No. MRC1+ TAMs/field
60
40
20
0
*
MRC1-/Lo MRC1+/Hi

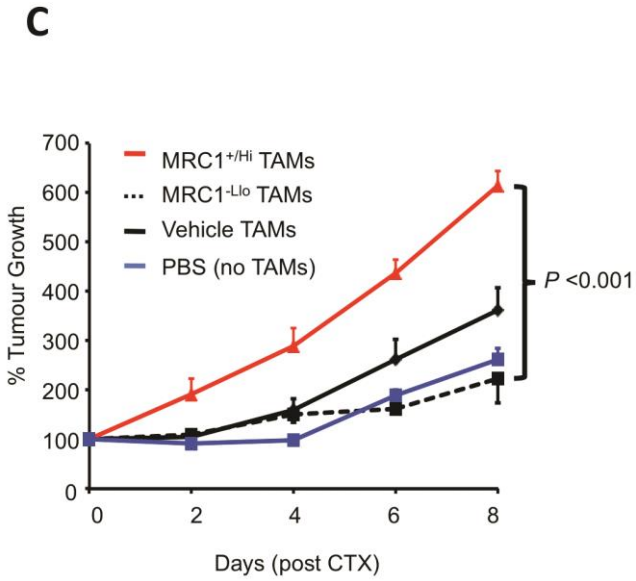
C
MRC1+/Hi TAMs
MRC1-Llo TAMs
Vehicle TAMs
PBS (no TAMs)
P <0.001
% Tumour Growth
700
600
500
400
300
200
100
0
0
2
4
6
8
Days (post CTX)

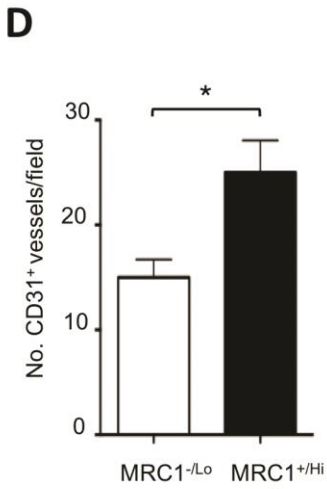
D
No. CD31+ vessels/field
30
20
10
0
*
MRC1-/Lo MRC1+/Hi

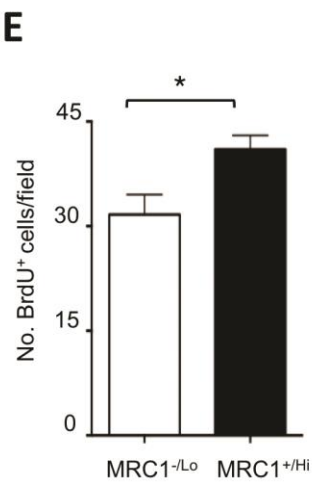
E
No. BrdU+ cells/field
45
30
15
0
*
MRC1-/Lo MRC1+/Hi

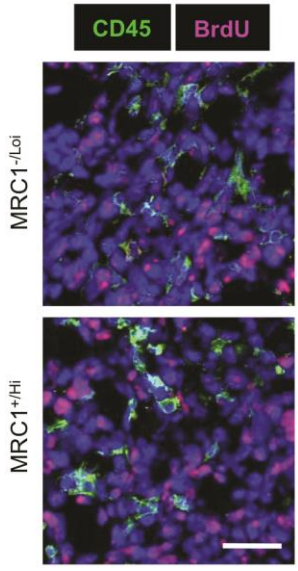
CD45
BrdU
MRC1-/Loi
MRC1+/Hi

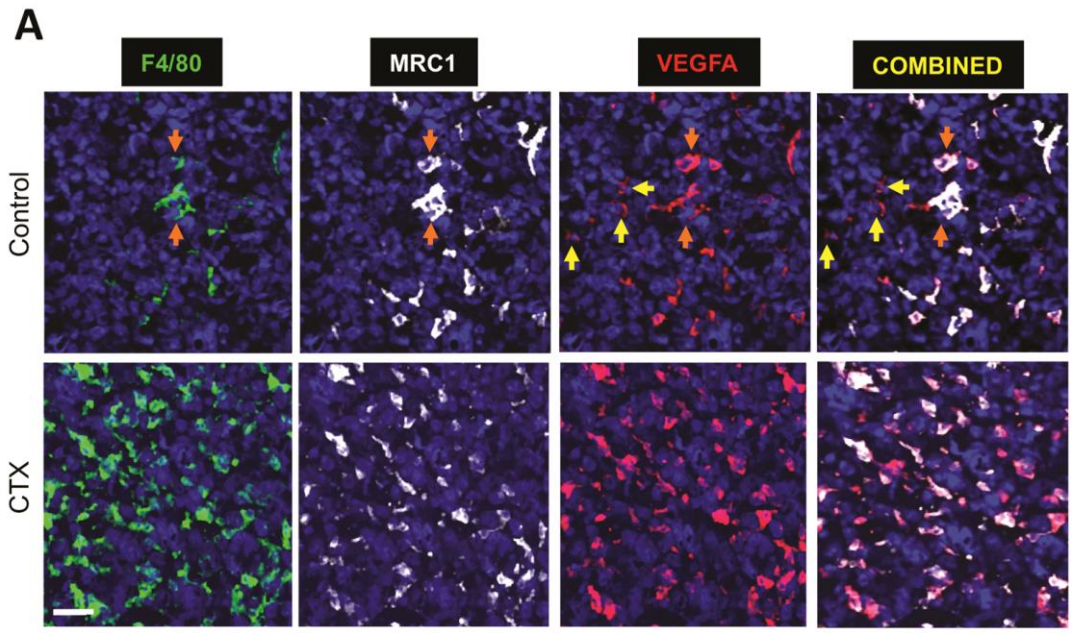
A
F4/80
MRC1
VEGFA
COMBINED
Control
CTX

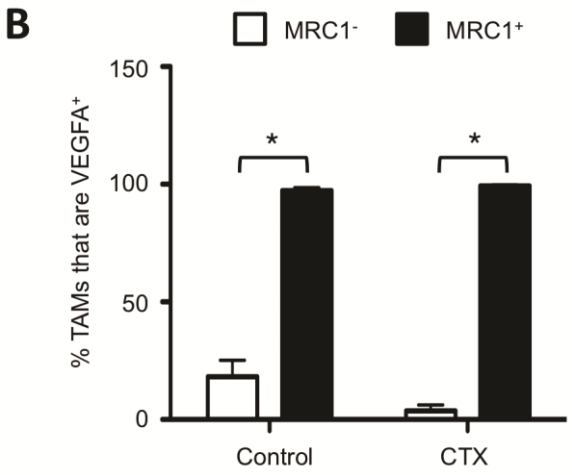
B
MRC1-
MRC1+
% TAMs that are VEGFA+
150
100
50
0
*
*
Control
CTX

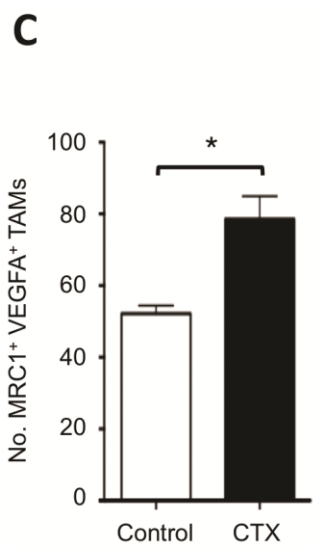
C
No. MRC1+ VEGFA+ TAMs
100
80
60
40
20
0
*
Control
CTX

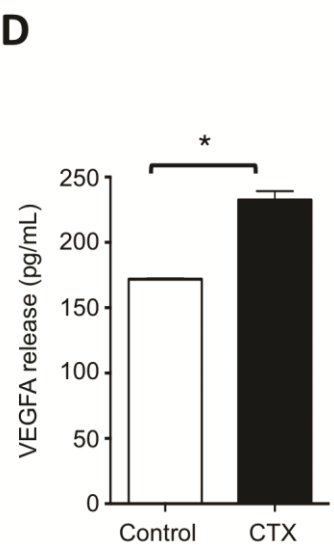
D
VEGFA release (pg/mL)
250
200
150
100
50
0
*
Control
CTX

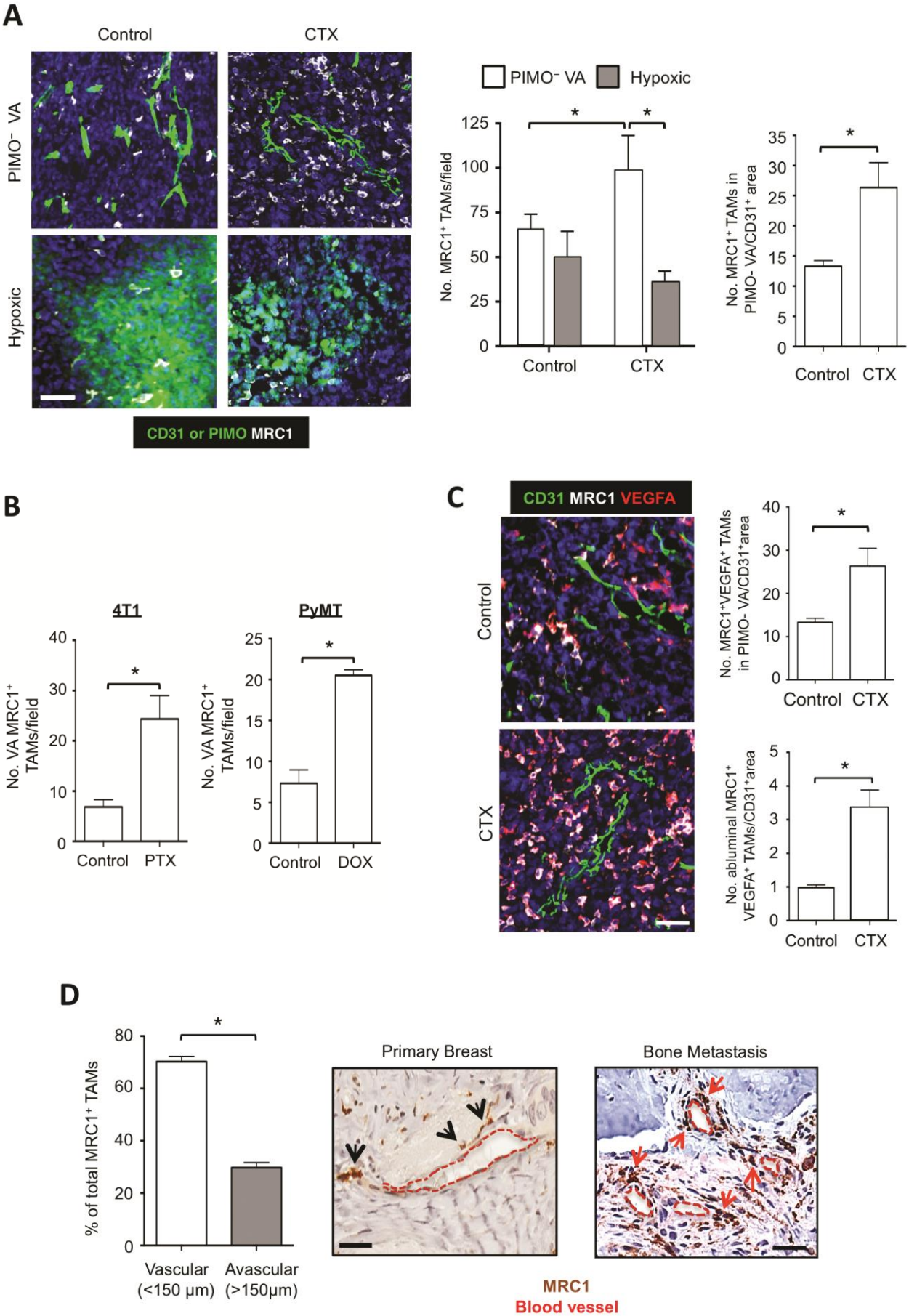
A
Control
CTX
PIMO⁻ VA
Hypoxic
CD31 or PIMO MRC1
PIMO⁻ VA
Hypoxic
No. MRC1⁺ TAMs/field
125
100
75
50
25
0
Control
CTX
No. MRC1⁺ TAMs in PIMO- VA/CD31⁺ area
35
30
25
20
15
10
5
0
Control
CTX
B
4T1
No. VA MRC1⁺ TAMs/field
40
30
20
10
0
Control
PTX
PyMT
No. VA MRC1⁺ TAMs/field
25
20
15
10
5
0
Control
DOX
C
CD31 MRC1 VEGFA
Control
CTX
No. MRC1⁺VEGFA⁺ TAMs in PIMO- VA/CD31⁺area
40
30
20
10
0
Control
CTX
No. abluminal MRC1⁺ VEGFA⁺ TAMs/CD31⁺area
5
4
3
2
1
0
Control
CTX
D
% of total MRC1⁺ TAMs
80
60
40
20
0
Vascular (<150 µm)
Avascular (>150µm)
Primary Breast
Bone Metastasis
MRC1
Blood vessel

Figure 5

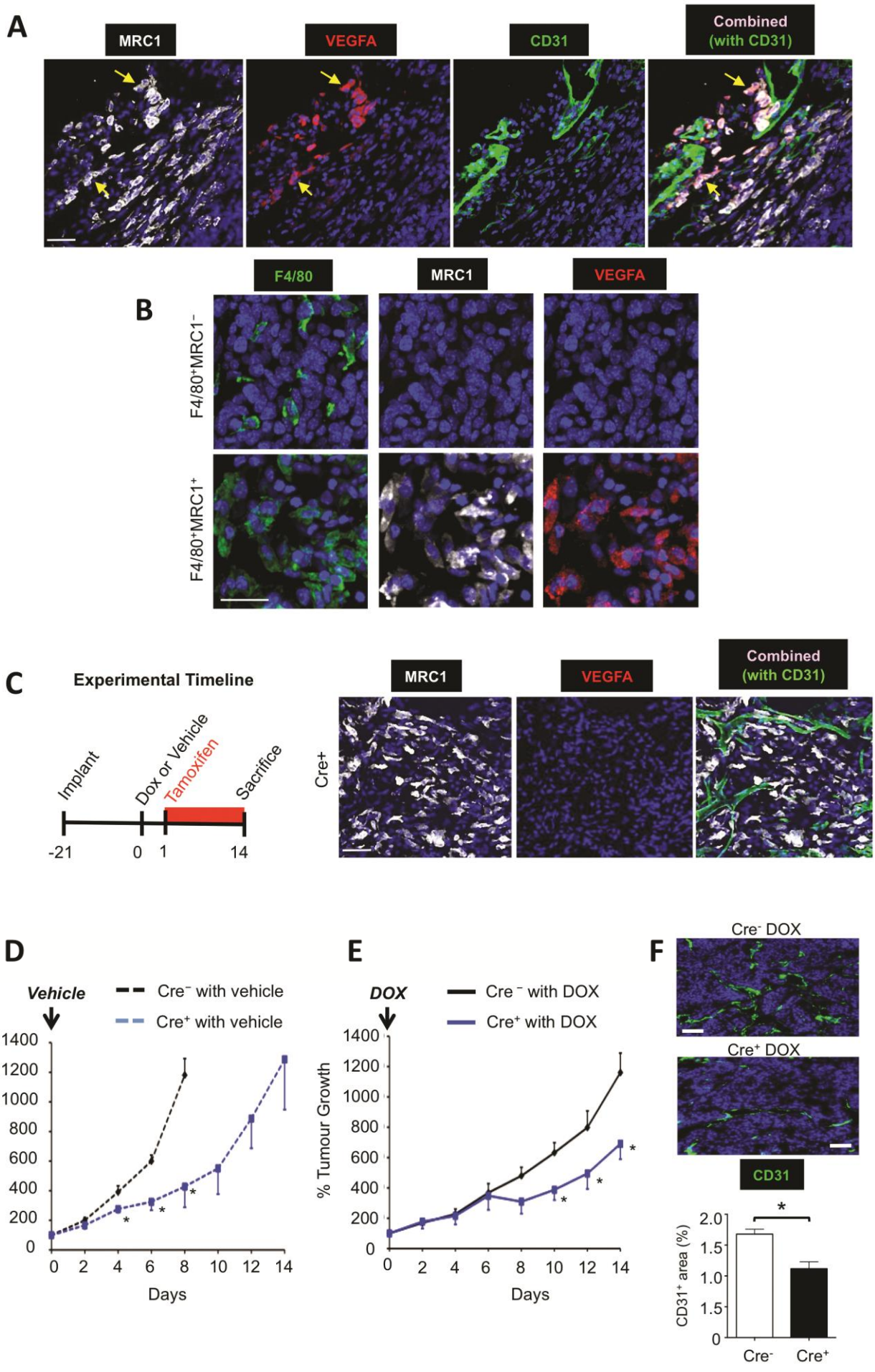
A
MRC1
VEGFA
CD31
Combined (with CD31)
B
F4/80
MRC1
VEGFA
F4/80+MRC1−
F4/80+MRC1+
C
Experimental Timeline
Implant
Dox or Vehicle
Tamoxifen
Sacrifice
-21
0
1
14
MRC1
VEGFA
Combined (with CD31)
Cre+
D
Vehicle
Cre− with vehicle
Cre+ with vehicle
% Tumour Growth
Days
E
DOX
Cre − with DOX
Cre+ with DOX
% Tumour Growth
Days
F
Cre- DOX
Cre+ DOX
CD31
CD31+ area (%)
Cre-
Cre+

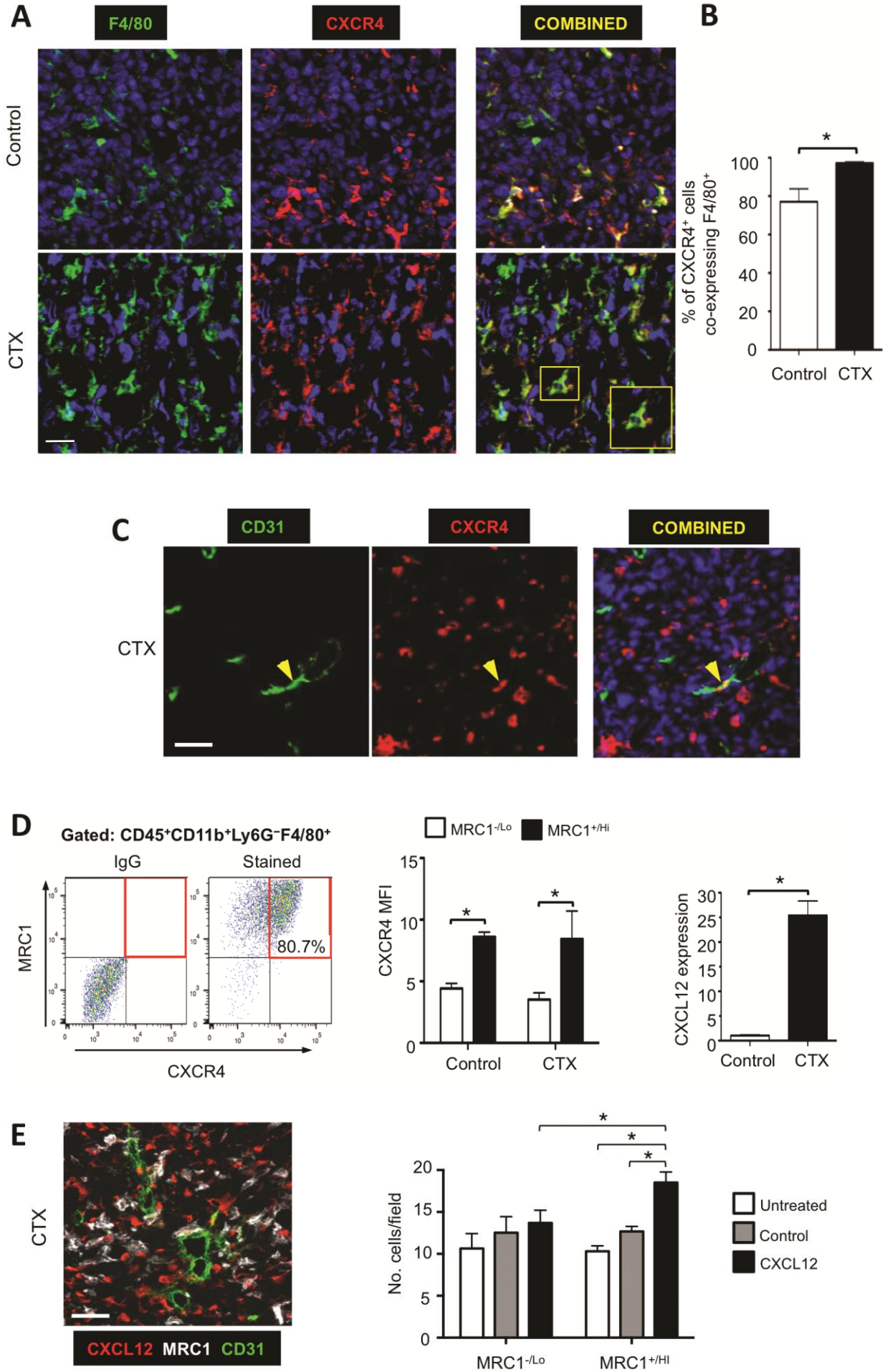
A
F4/80
CXCR4
COMBINED
Control
CTX
B
% of CXCR4+ cells co-expressing F4/80+
100
80
60
40
20
0
Control
CTX
*
C
CD31
CXCR4
COMBINED
CTX
D
Gated: CD45+CD11b+Ly6G−F4/80+
IgG
Stained
MRC1
CXCR4
80.7%
MRC1-/Lo
MRC1+/Hi
CXCR4 MFI
15
10
5
0
Control
CTX
CXCL12 expression
30
25
20
15
10
5
0
E
CTX
CXCL12 MRC1 CD31
No. cells/field
20
15
10
5
0
MRC1-/Lo
MRC1+/HI
Untreated
Control
CXCL12

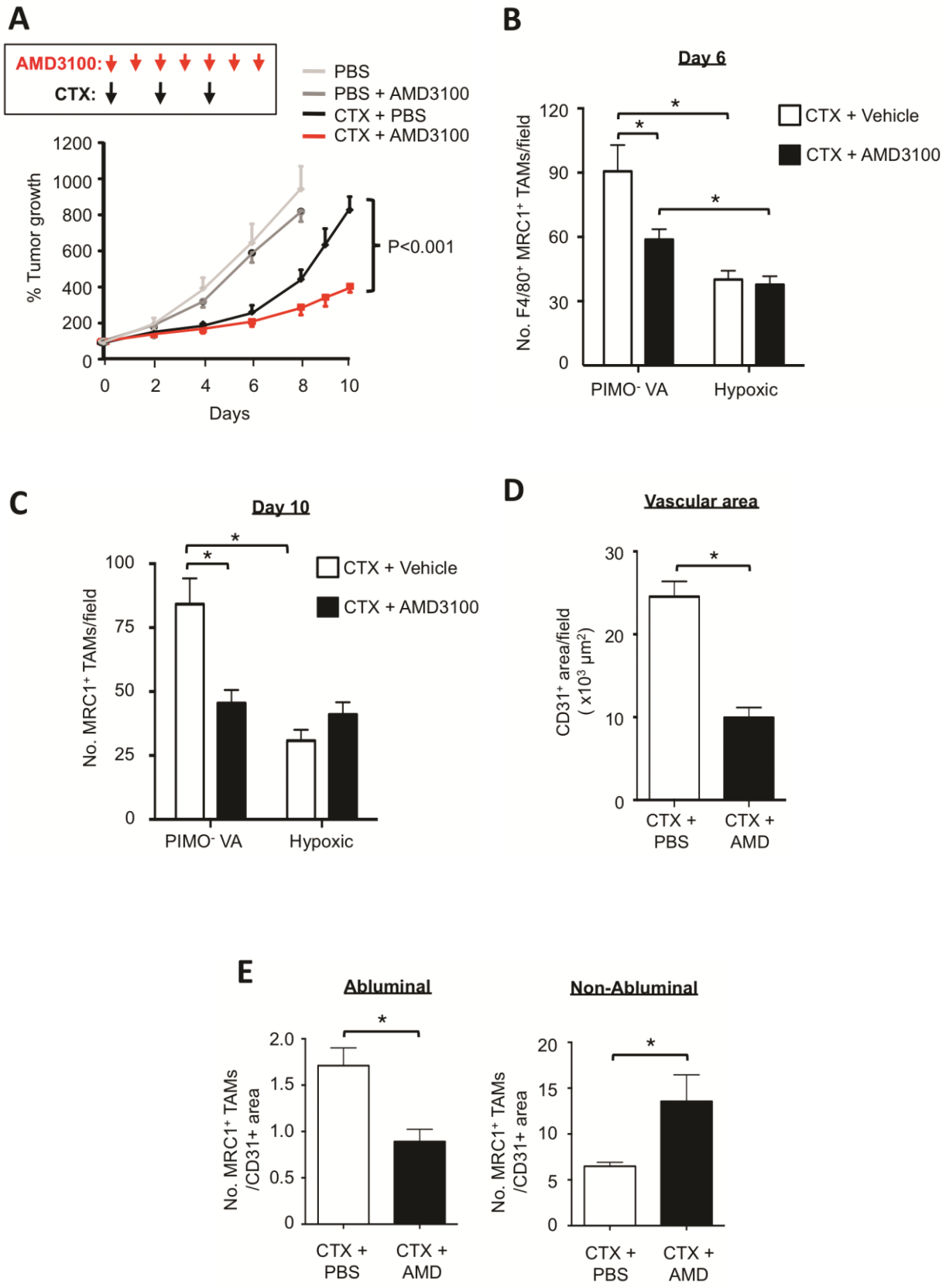
A
AMD3100:
CTX:
PBS
PBS + AMD3100
CTX + PBS
CTX + AMD3100
% Tumor growth
1200
1000
800
600
400
200
0
0
2
4
6
8
10
Days
P<0.001
B
Day 6
No. F4/80+ MRC1+ TAMs/field
120
90
60
30
0
CTX + Vehicle
CTX + AMD3100
PIMO- VA
Hypoxic
C
Day 10
No. MRC1+ TAMs/field
100
75
50
25
0
CTX + Vehicle
CTX + AMD3100
PIMO- VA
Hypoxic
D
Vascular area
CD31+ area/field
(x10³ µm²)
30
20
10
0
CTX + PBS
CTX + AMD
E
Abluminal
No. MRC1+ TAMs /CD31+ area
2.0
1.5
1.0
0.5
0
CTX + PBS
CTX + AMD
Non-Abluminal
No. MRC1+ TAMs /CD31+ area
20
15
10
5
0
CTX + PBS
CTX + AMD

Figure S1. Effects of various cytotoxic agents on TAM accumulation in three mouse tumor models. (**A**) $CD31^+$ vessel length and the % of tumor areas that were $PIMO^+$ in control and CTX-treated LLC1 tumors 48 h after the last injection of CTX (day 6) (n = 6-12/group). (**B**) Gating strategy for flow cytometric analysis of the proportion of $CD45^+$ $CD11b^+$ $Ly6G^-$ $F4/80^+$ TAMs (expressed as a % of viable $CD45^+$ leukocytes). Dispersed LLC1s were gated on viable cells (1) followed by the pan-leukocyte marker CD45 (2). Neutrophils were identified and excluded from further analyses by gating on $CD11b^+$ $Ly6G^-$ cells (3). Finally, mature macrophages were identified on the basis of $Ly6C^{HI}$ $F4/80^{Hi}$ marker profile (n = 5-6/group). (**C**) Immunofluorescent quantification of $F4/80^+$ TAMs in control and CTX-treated LLCs (n = 7-8/group), control and PTX-treated orthotopic 4T1s (n= 8-9/group), and control and DOX-treated orthotopic MMTV-PyMT tumors (n = 7/group). (**D**) $F4/80^+$ $MRC1^+$ TAM numbers in $CD31^+$ vessel-associated areas in control and PTX-treated orthotopic 4T1 tumors (n = 8-9/group) or control and DOX-treated orthotopic MMTV-PyMT tumors (n = 8-9/group). The 'Control' group in each case is the vehicle for the cytotoxic agent. *P<0.05.

Figure S2. Further Characterization of MRC1+ TAMs in mouse tumors. (**A**) Co-localization of MRC1 with F4/80 in LLC1 (n = 4-6/group), 4T1 (n = 5-6/group) and MMTV-PyMT tumors (n = 4/group). (**B**) Immunofluorescent labelling of BrdU and MRC1 (n = 4/group) or the (**C**) HSC markers, c-kit or Sca-1 (although occasional, single $Sca\text{-}1^+$ cells were evident) in tumors 48 h after the last injection of CTX. *P<0.05. Bars = 50 μm.

Figure S3. VEGFA Immunofluorescence in control and CTX-treated LLC1 tumors. (**A**) Representative immunostaining of VEGFA and $MRC1^+$ TAMs in vascularised, $PIMO^-$ VA and $PIMO^+$ (hypoxic) areas of control and CTX-treated tumors. (**B**) The proportion VEGF-expressing cells that were either $MRC1^-$ cells (ie.

non-TAMs) (left) or MRC1$^+$ TAMs (right) in the above areas. (**C**) These MRC1+ cells were not MDSCs as immature, 'monocytic MDSCs' (CD45$^+$CD11b$^+$Ly6G$^-$Ly6C$^+$ cells) and granulocytic MDSCs (CD45$^+$CD11b$^+$Ly6G$^+$ cells) were depleted in CTX-treated tumours. Also immature, 'monocytic MDSCs' from these tumors expressed very low levels of MRC1 (lower panels). *P<0.05.

Figure S4. Role of hypoxic (ie. HIF-expressing) TAMs in relapse of LLC1 tumors after CTX. (A) Immunofluorescence staining of MRC1$^+$ TAMs in PIMO$^+$ (hypoxic) areas of tumors 48h after CTX treatment (ie. prior to the start of tumor regrowth). Bar=50 μm. (B) Quantification of MRC1$^+$ TAM numbers in the PIMO$^+$ and PIMO$^-$ areas of WT, HIF1^{KO} and HIF2^{KO} tumors (n = 5/group). (C) Growth of tumors of WT, HIF1^{KO} (*left)* and HIF2^{KO} (*right*) mice showing the initial response of to CTX administration (3 black arrows), or their subsequent relapse (n = 3-5 mice/group at endpoint). (D) Immunohistochemical labelling of HIF-1α and HIF-2α in TAMs in vehicle-treated tumors confirmed the Lys-Cre deletion of these genes in HIF-1 and 2α ko mice.

Figure S5. Effect of CXCR4 blockade on various tumor parameters in CTX-treated LLC1 tumors. (**A**) The number of MRC1$^+$ TAMs in PIMO–VA vs. hypoxic regions and representative images of VEGF expression by MRC1$^+$ TAMs in PIMO–VA regions of CTX-treated tumours 48hr after the last dose and following relapse. (**B**) The number of MRC1$^-$ TAMs in well-vascularised PIMO$^-$ VA and hypoxic, PIMO$^+$ areas of tumors given CTX in combination with saline or AMD3100 was quantified by immunofluorescence staining at 6 days post-therapy. (**C**) Quantification of CD31$^+$ vessels length, the % PIMO$^+$ tumor area and the numbers of BrdU$^+$ proliferating cells in tumors from mice, 6 days after administration of either CTX + vehicle (PBS) or CTX + AMD3100. *P<0.05.

Figure S6. **Co-localization of HIFs 1 and 2, but not CXCL12 or HO-1, with hypoxia in LLC1s**. (**A**) Representative staining of: (i) HIF-1α in paraffin-wax sections or (ii) HIF-2α in frozen sections of LLC1 tumors (top panels). HIF-1α expression was widespread in PBS-treated control tumors whereas HIF-2α was upregulated in hypoxic areas. Both α subunits were reduced after CTX. (**B**) CXCL12 is found mainly in hypoxic areas of control LLC1s, but expressed in both normoxic and hypoxic tumor areas after CTX. (**C**) The oxidative stress marker, HMOX-1, was upregulated in $PIMO^-$ CXCL12-rich perivascular areas of CTX-treated tumours (i & ii) where it was expressed by both $MRC1^+$ and $MRC1^-$ cells (white or yellow arrows respectively) (iii). Bars=50μm *P<0.05.

Figure S7. **Effect of CXCR4 blockade on the longer-term re-growth kinetics of primary and metastatic LLC1s**. Extending the relapse period of mice treated with PBS, AMD3100, CTX or CTX+ AMD3100 showed that neither primary tumors (**A**) nor their pulmonary metastases (**B**) had accelerated regrowth (ie. rebounded) after cessation of the AMD3100 treatment.

Figure S1

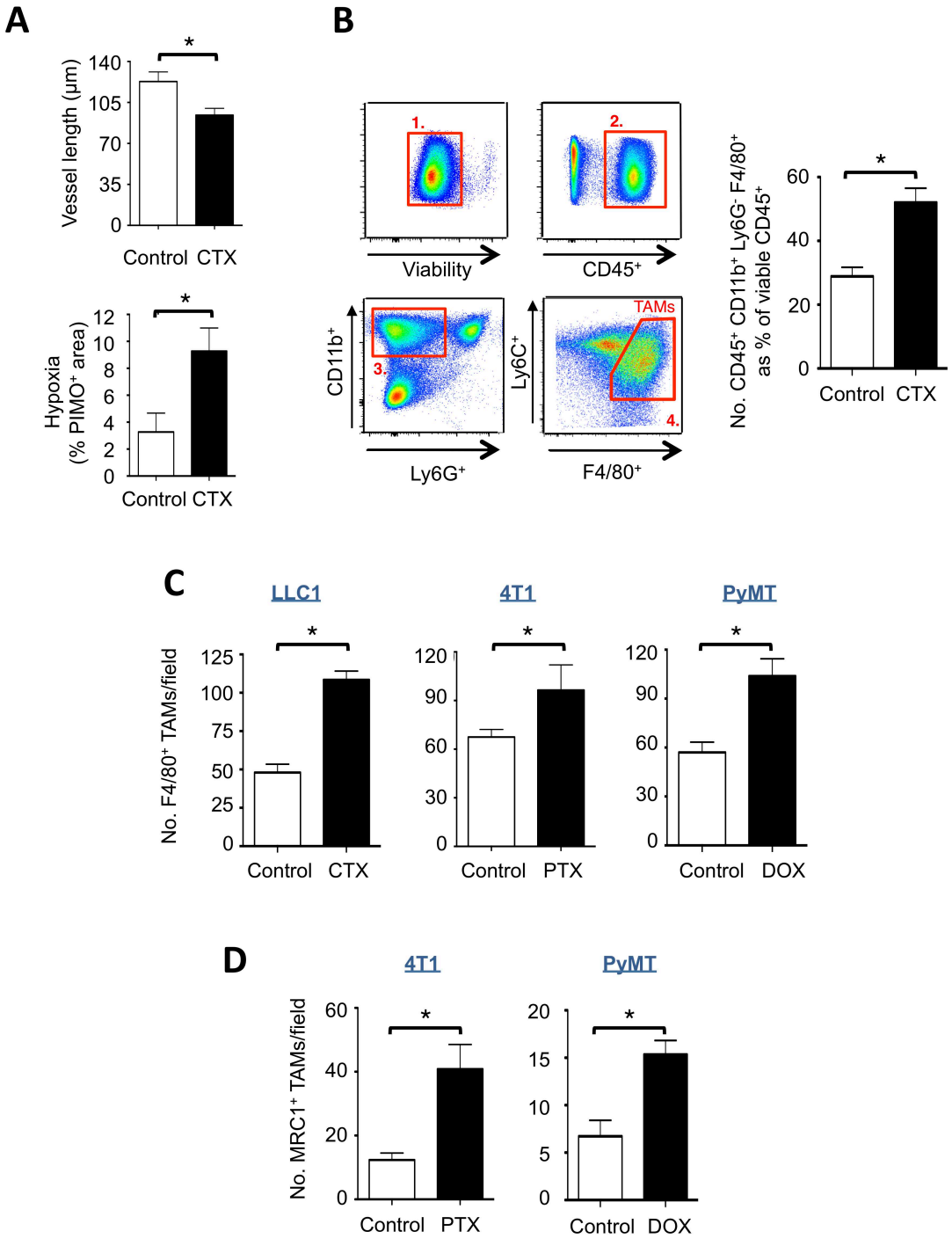
A
Vessel length (µm)
140
105
70
35
0
Control CTX
*
Hypoxia (% PIMO+ area)
12
10
8
6
4
2
0
Control CTX
*
B
1.
Viability
2.
CD45+
CD11b+
3.
Ly6G+
Ly6C+
TAMs
4.
F4/80+
No. CD45+ CD11b+ Ly6G- F4/80+ as % of viable CD45+
60
40
20
0
Control CTX
*
C
LLC1
4T1
PyMT
No. F4/80+ TAMs/field
125
100
75
50
25
0
Control CTX
120
90
60
30
0
Control PTX
Control DOX
D
4T1
PyMT
No. MRC1+ TAMs/field
60
40
20
0
Control PTX
20
15
10
5
0
Control DOX

Figure S2

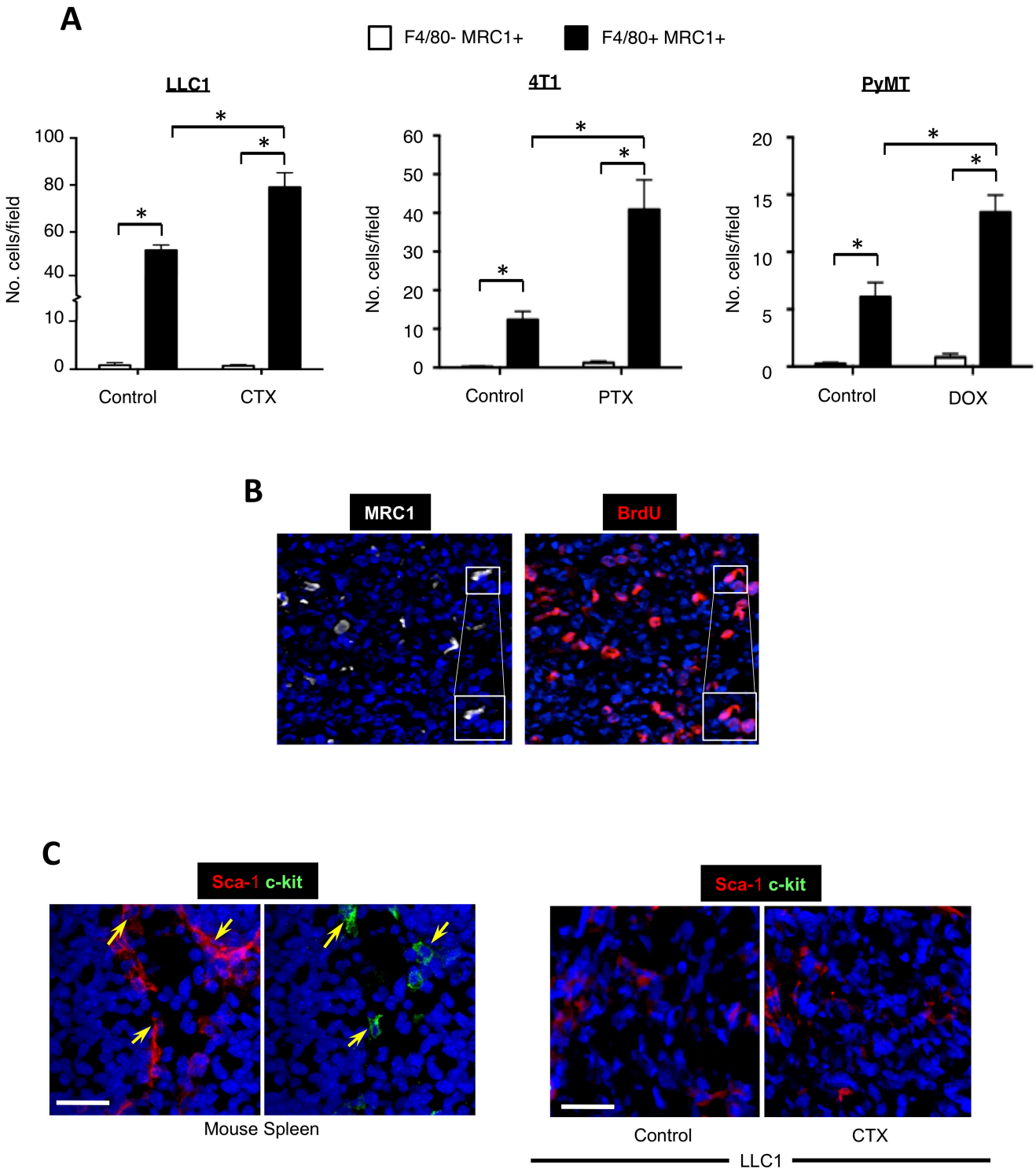
A
F4/80- MRC1+
F4/80+ MRC1+
LLC1
4T1
PyMT
No. cells/field
Control
CTX
PTX
DOX
B
MRC1
BrdU
C
Sca-1 c-kit
Mouse Spleen
Control
CTX
LLC1

Figure S3

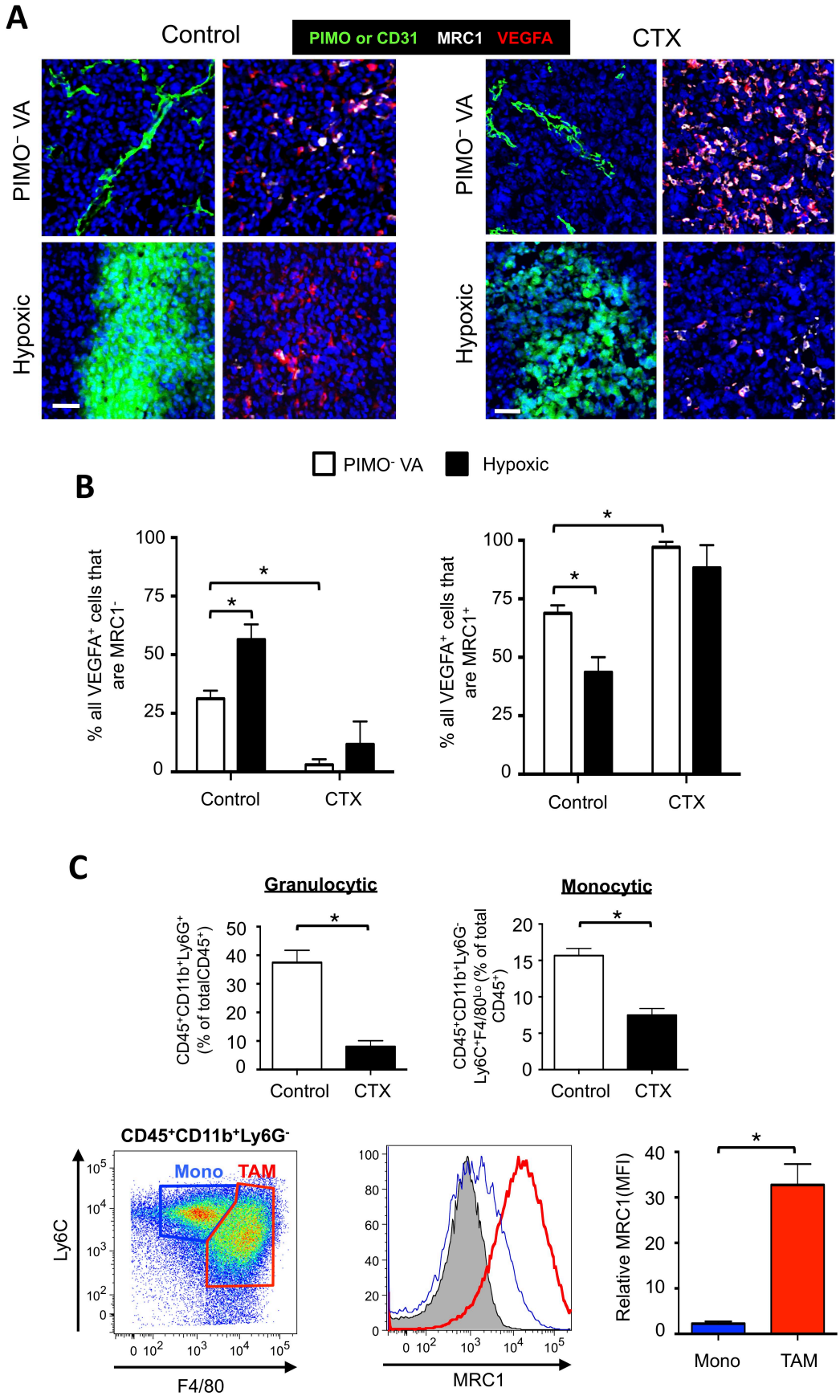
A
Control
PIMO or CD31 MRC1 VEGFA
CTX
PIMO⁻ VA
Hypoxic
PIMO⁻ VA
Hypoxic
B
PIMO⁻ VA
Hypoxic
% all VEGFA⁺ cells that are MRC1⁻
100
75
50
25
0
Control
CTX
% all VEGFA⁺ cells that are MRC1⁺
100
75
50
25
0
Control
CTX
C
Granulocytic
CD45⁺CD11b⁺Ly6G⁺ (% of totalCD45⁺)
50
40
30
20
10
0
Control
CTX
Monocytic
CD45⁺CD11b⁺Ly6G⁻ Ly6C⁺F4/80ˡᵒ (% of total CD45⁺)
20
15
10
5
0
Control
CTX
CD45⁺CD11b⁺Ly6G⁻
Mono
TAM
Ly6C
F4/80
MRC1
Relative MRC1(MFI)
40
30
20
10
0
Mono
TAM

Figure S4

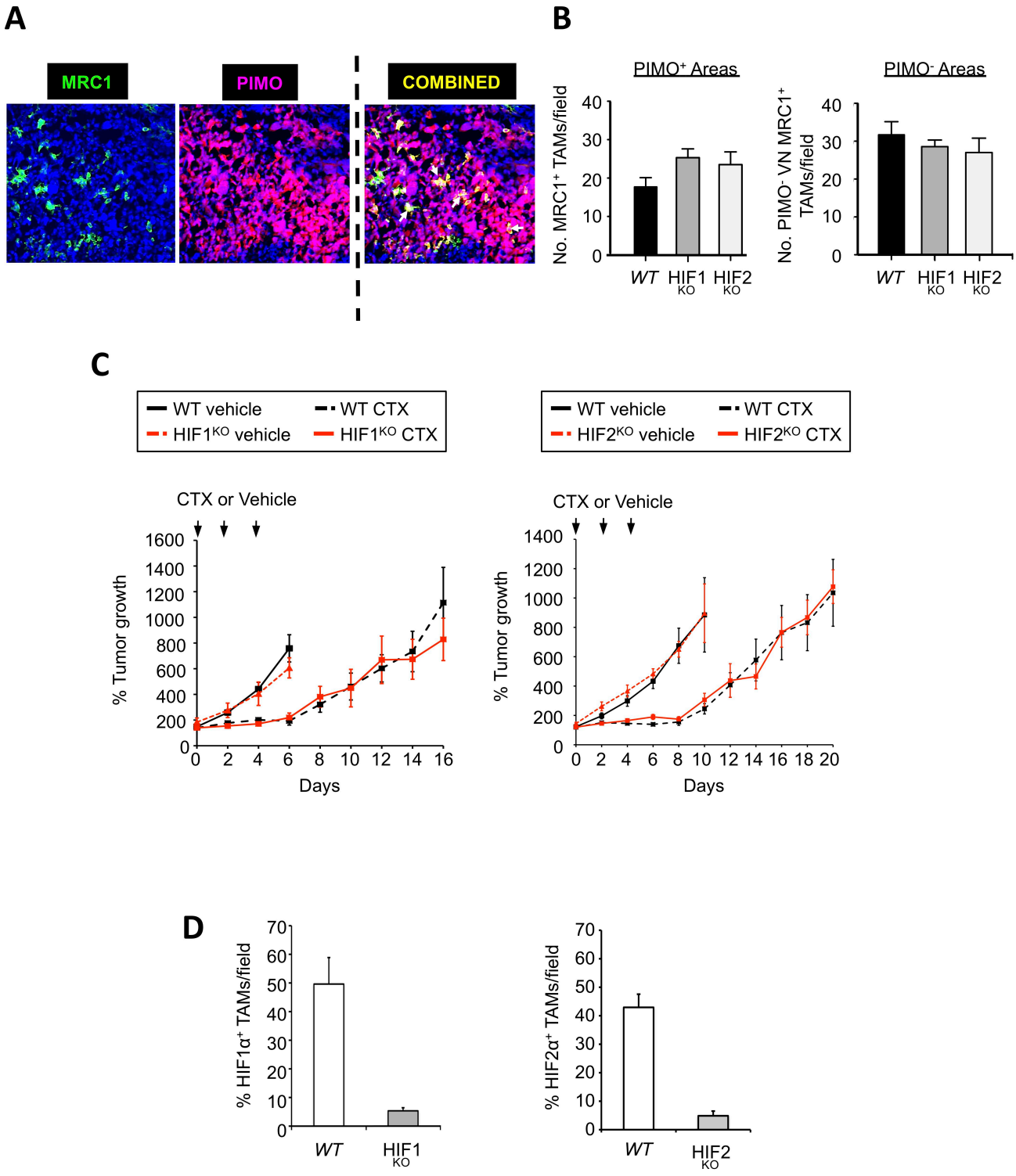
A
MRC1
PIMO
COMBINED
B
PIMO+ Areas
PIMO- Areas
No. MRC1+ TAMs/field
No. PIMO- VN MRC1+ TAMs/field
WT
HIF1 KO
HIF2 KO
C
WT vehicle
WT CTX
HIF1KO vehicle
HIF1KO CTX
HIF2KO vehicle
HIF2KO CTX
CTX or Vehicle
% Tumor growth
Days
D
% HIF1α+ TAMs/field
% HIF2α+ TAMs/field

Figure S5

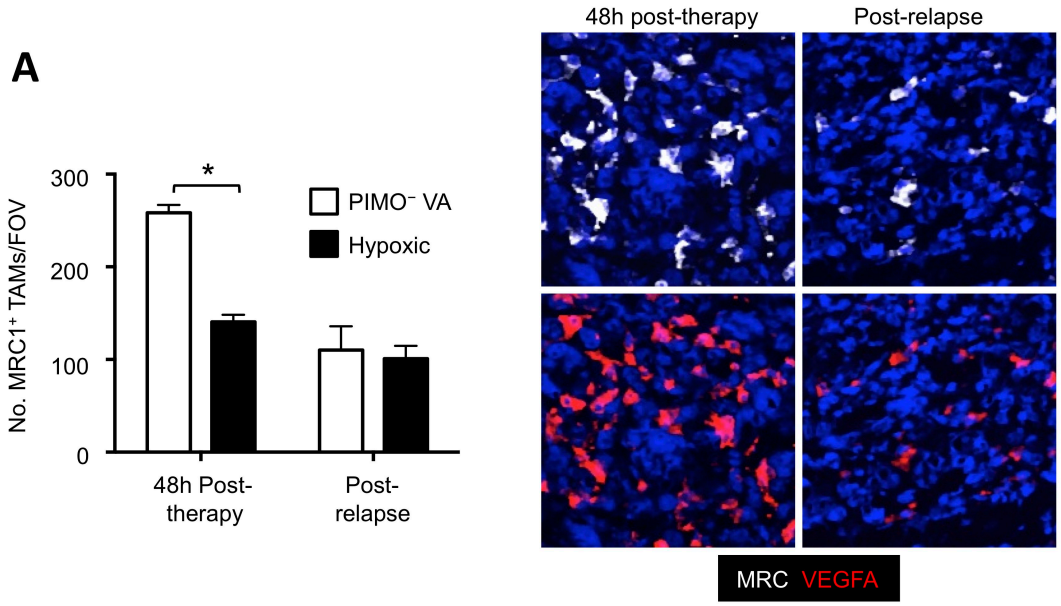
A
48h post-therapy
Post-relapse
No. MRC1+ TAMs/FOV
300
200
100
0
*
PIMO- VA
Hypoxic
48h Post-therapy
Post-relapse
MRC VEGFA

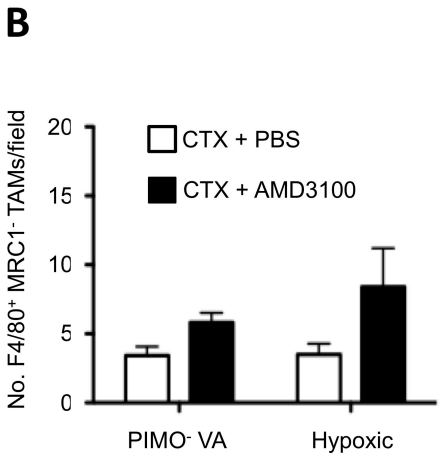
B
No. F4/80+ MRC1- TAMs/field
20
15
10
5
0
CTX + PBS
CTX + AMD3100
PIMO- VA
Hypoxic

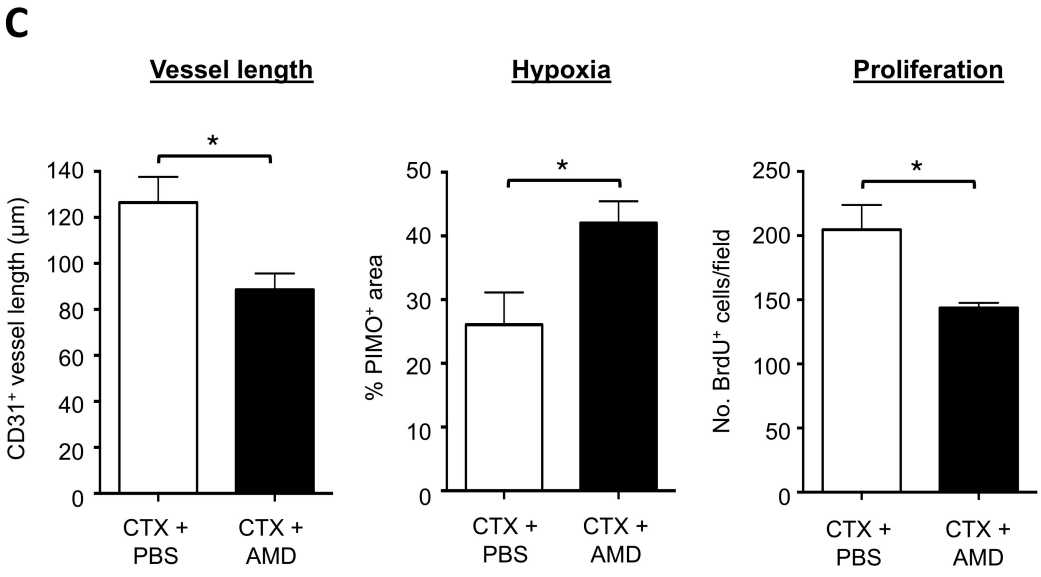
C
Vessel length
Hypoxia
Proliferation
CD31+ vessel length (µm)
140
120
100
80
60
40
20
0
*
CTX + PBS
CTX + AMD
% PIMO+ area
50
40
30
20
10
0
*
CTX + PBS
CTX + AMD
No. BrdU+ cells/field
250
200
150
100
50
0
*
CTX + PBS
CTX + AMD

Figure S6

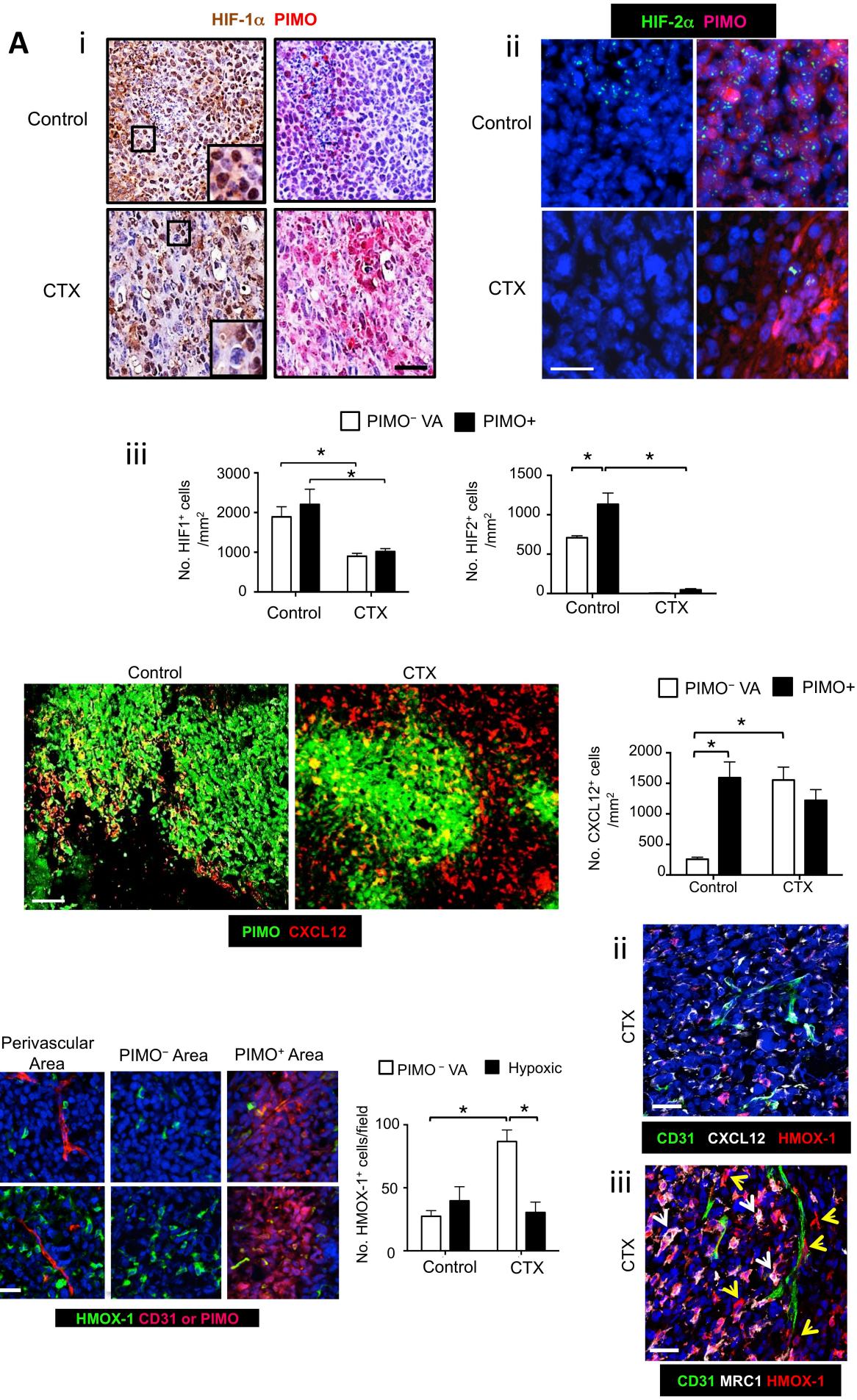
A
i
HIF-1α PIMO
Control
CTX
ii
HIF-2α PIMO
Control
CTX
iii
PIMO⁻ VA
PIMO+
No. HIF1⁺ cells /mm²
3000
2000
1000
0
Control
CTX
No. HIF2⁺ cells /mm²
1500
1000
500
0
Control
CTX
B
Control
CTX
PIMO CXCL12
PIMO⁻ VA
PIMO+
No. CXCL12⁺ cells /mm²
2000
1500
1000
500
0
Control
CTX
C
i
Perivascular Area
PIMO⁻ Area
PIMO⁺ Area
Control
CTX
HMOX-1 CD31 or PIMO
PIMO⁻ VA
Hypoxic
No. HMOX-1⁺ cells/field
100
50
0
Control
CTX
ii
CTX
CD31 CXCL12 HMOX-1
iii
CTX
CD31 MRC1 HMOX-1

Figure S7

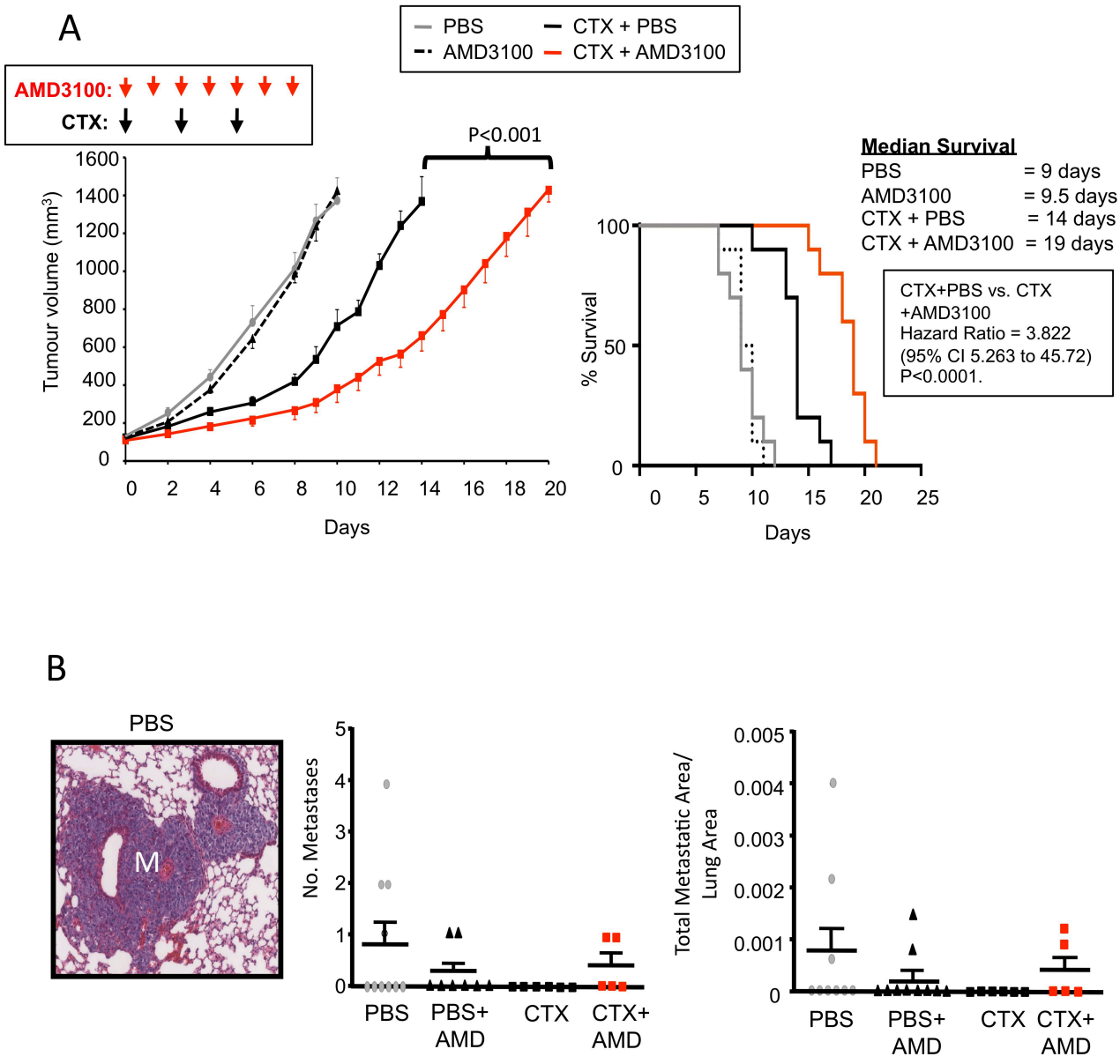
A
PBS
AMD3100
CTX + PBS
CTX + AMD3100
AMD3100:
CTX:
P<0.001
Tumour volume (mm3)
Days
% Survival
Median Survival
PBS = 9 days
AMD3100 = 9.5 days
CTX + PBS = 14 days
CTX + AMD3100 = 19 days
CTX+PBS vs. CTX +AMD3100
Hazard Ratio = 3.822
(95% CI 5.263 to 45.72)
P<0.0001.
B
PBS
M
No. Metastases
Total Metastatic Area/ Lung Area
PBS
PBS+ AMD
CTX
CTX+ AMD